

RESEARCH ARTICLE

10.1002/2015JA022244

Stepwise tailward retreat of magnetic reconnection: THEMIS observations of an auroral substorm

Key Points:

- Auroral stepwise poleward expansions were associated with reconnection stepwise tailward retreat
- This spatially stepwise association is consequence of magnetic flux pileup
- The stepwise association resolved objections to the Hones poleward leap concept

Correspondence to:

A. Ieda,
ieda@nagoya-u.jp

Citation:

Ieda, A., et al. (2016), Stepwise tailward retreat of magnetic reconnection: THEMIS observations of an auroral substorm, *J. Geophys. Res. Space Physics*, 121, 4548–4568, doi:10.1002/2015JA022244.

Received 4 DEC 2015

Accepted 26 APR 2016

Accepted article online 2 MAY 2016

Published online 28 MAY 2016

A. Ieda¹, Y. Nishimura², Y. Miyashita¹, V. Angelopoulos³, A. Runov³, T. Nagai⁴, H. U. Frey⁵, D. H. Fairfield⁶, J. A. Slavin⁷, H. Vanhamäki⁸, H. Uchino^{1,9}, R. Fujii¹, Y. Miyoshi¹, and S. Machida¹

¹Institute for Space-Earth Environmental Research, Nagoya University, Nagoya, Japan, ²Department of Atmospheric and Oceanic Sciences, University of California, Los Angeles, California, USA, ³Department of Earth and Space Sciences, University of California, Los Angeles, California, USA, ⁴Department of Earth and Planetary Sciences, Tokyo Institute of Technology, Tokyo, Japan, ⁵Space Sciences Laboratory, University of California, Berkeley, California, USA, ⁶Heliophysics Science Division, NASA Goddard Space Flight Center, Greenbelt, Maryland, USA, ⁷Department of Atmospheric, Oceanic and Space Sciences, University of Michigan, Ann Arbor, Michigan, USA, ⁸Department of Physics, University of Oulu, Oulu, Finland, ⁹Graduate School of Science, Kyoto University, Kyoto, Japan

Abstract Auroral stepwise poleward expansions were clarified by investigating a multiple-onset substorm that occurred on 27 February 2009. Five successive auroral brightenings were identified in all-sky images, occurring at approximately 10 min intervals. The first brightening was a faint precursor. The second brightening had a wide longitude; thus, it represented the Akasofu substorm onset. Other brightenings expanded poleward; thus, they were interpreted to be auroral breakups. These breakups occurred stepwise; that is, later breakups were initiated at higher latitudes. Corresponding reconnection signatures were studied using Time History of Events and Macroscale Interactions during Substorms (THEMIS) satellite observations between 8 and 24 R_E down the magnetotail. The Akasofu substorm onset was not accompanied by a clear reconnection signature in the tail. In contrast, the three subsequent auroral breakups occurred simultaneously (within a few minutes) with three successive fast flows at 24 R_E ; thus, these were interpreted to be associated with impulsive reconnection episodes. These three fast flows consisted of a tailward flow and two subsequent earthward flows. The flow reversal at the second breakup indicated that a tailward retreat of the near-Earth reconnection site occurred during the substorm expansion phase. In addition, the earthward flow at the third breakup was consistent with the classic tailward retreat near the end of the expansion phase; therefore, the tailward retreat is likely to have occurred in a stepwise manner. We interpreted the stepwise characteristics of the tailward retreat and poleward expansion to be potentially associated by a stepwise magnetic flux pileup.

1. Introduction

Substorms are an explosive release of energy from the magnetotail into the polar ionosphere. Akasofu [1964] defined substorm onset as a sudden auroral brightening with a wide longitude (i.e., “initial brightening”). This onset is followed by an auroral poleward expansion (i.e., “auroral breakup”) and further auroral activations. However, how this auroral sequence is spatially associated with disturbances in the magnetotail has remained unclear.

The near-Earth neutral line (NENL) model of substorms assumes that magnetic reconnections at around 20 R_E down the tail are the dominant substorm mechanism [Coppi et al., 1966; Atkinson, 1966; Hones et al., 1973; Nishida and Nagayama, 1973; Russell and McPherron, 1973; Hones, 1976; Baker et al., 1996; Sergeev et al., 2012]. Reconnection-associated fast plasma flows tend to be observed in the magnetotail near the time of substorm onset [Hones et al., 1984; Moldwin and Hughes, 1993; Nagai et al., 1998; Miyashita et al., 2009; Machida et al., 2014]. Such flows are almost always observed beyond 25 R_E down the tail by spacecraft near the longitude of auroral breakup, indicating that magnetic reconnection in the tail is a necessary condition for substorm development [Ieda et al., 2008].

However, so far the NENL model has not well explained ionospheric disturbances, which are typically more complex, especially during multiple-onset substorms. Auroras and westward electrojet currents (WEJ) often include multiple onsets during the substorm expansion phase [Pytte et al., 1976a; Rostoker et al., 1980].

In addition, auroral poleward expansions sometimes occur stepwise; that is, they start at successively higher and higher latitudes at approximately 10 min intervals [Kisabeth and Rostoker, 1971, 1974; Wiens and Rostoker, 1975; Sergeev and Yahnin, 1979; Aikio et al., 2006]. It remains unclear in the context of the NENL model how to understand such discrete events.

The key to understanding multiple onset substorms is the clarification of the tailward retreat of the neutral line. Classically, the NENL does not move significantly during the substorm expansion phase [Nishida and Nagayama, 1973], even with multiple onsets [Pytte et al., 1976a], but suddenly retreats tailward at the beginning of the substorm recovery phase [Hones et al., 1973; Baumjohann et al., 1999].

Hones et al. [1973] associated such a sudden tailward retreat with an auroral jump into the polar cap as follows. By the classical definition, the WEJ starts to subside at auroral latitudes ($\sim 65\text{--}70^\circ$ in magnetic latitude; MLAT) around the beginning of the substorm recovery phase. Around this time, Hones et al. [1973] observed that the WEJ begins to develop at polar cap latitudes (~ 74 MLAT). They termed this phenomenon the “poleward leap” of the principal current of the auroral WEJ. This poleward leap was interpreted as the ionospheric signature of the tailward retreat of the neutral line [Hones et al., 1973; Hones, 1979, 1992]. This poleward leap concept completes the ionospheric aspects of the classic NENL model of substorm. In other words, the classic NENL model predicts two auroral breakups, one corresponds to the substorm onset and the other to the poleward leap (i.e., tailward retreat); although, the latter feature has not been appreciated in later studies. Note that the classic NENL model includes only one “poleward leap.”

However, sometimes, more than two discrete poleward expansions of WEJ and auroras are observed in the ionosphere during substorms [e.g., Kisabeth and Rostoker, 1971; Sergeev and Yahnin, 1979]. For this and other reasons, the poleward leap concept has been rejected [e.g., Rostoker, 1986; Craven and Frank, 1987; Opgenoorth et al., 1994; Elphinstone et al., 1996; Mende et al., 1999]. Thus, the NENL model has not been successful in explaining ionospheric disturbances, especially during multiple-onset substorms.

The purpose of this study was to clarify reconnection signatures corresponding to stepwise poleward expansions. We studied a multiple-onset substorm with five major brightenings using satellite and ground-based observations. The results indicate that stepwise poleward expansion is associated with stepwise tailward retreat that starts during the substorm expansion phase. This finding advances the poleward leap concept by allowing stepwise retreat in order to explain more than two breakups even when such breakups start at successively higher and higher latitudes. We further interpreted this spatial association as due to stepwise magnetic flux pileup near the Earth. Such stepwise tailward retreat is probably evident only when auroral poleward expansions are stepwise.

2. Data Set

2.1. THEMIS Satellites

The primary data for this study were collected by the Time History of Events and Macroscale Interactions during Substorms (THEMIS) mission [Angelopoulos, 2008], including both satellite and ground-based observations. The five identical THEMIS satellites were launched on 17 February 2007: TH1, TH2, TH3, TH4, and TH5. We used spin-resolution (~ 3 s) magnetic field and plasma data. The magnetic field data were from the THEMIS flux gate magnetometer (FGM) [Auster et al., 2008]. Ions and electrons were measured by the top-hat electrostatic analyzer (ESA) [McFadden et al., 2008] and the solid state telescope (SST) [Angelopoulos, 2008]. The ESA measures thermal particles from 5 to 25 keV (ions) and up to 32 keV (electrons). The SST measures energetic particles from 25 keV to 6 MeV (ions) and up to 1 MeV (electrons). The ion velocity moments were calculated by merging ESA and SST data. The electron pressure was calculated from ESA electron data.

2.2. Satellite Locations and Coordinates

The aberrated geocentric solar magnetospheric (AGSM) coordinate system was adopted with an angle of 4° for satellite locations (Figure 1) and data. The Z locations were also calculated relative to a neutral sheet model [Tsyganenko and Fairfield, 2004]. The magnetic latitude in degrees (MLAT) and the magnetic local time in hours (MLT) were calculated in the modified magnetic apex coordinates [Richmond, 1995] for a reference altitude of 110 km.

The magnetic foot point at 110 km altitude was calculated for the satellites by tracing a geomagnetic field line using the Tsyganenko 96 (T96) [Tsyganenko and Stern, 1996] and IGRF-11 [Finlay et al., 2010] models. The T96 input parameters included solar wind data (the dynamic pressure, B_y , and B_z) and the $SYM-H$ index

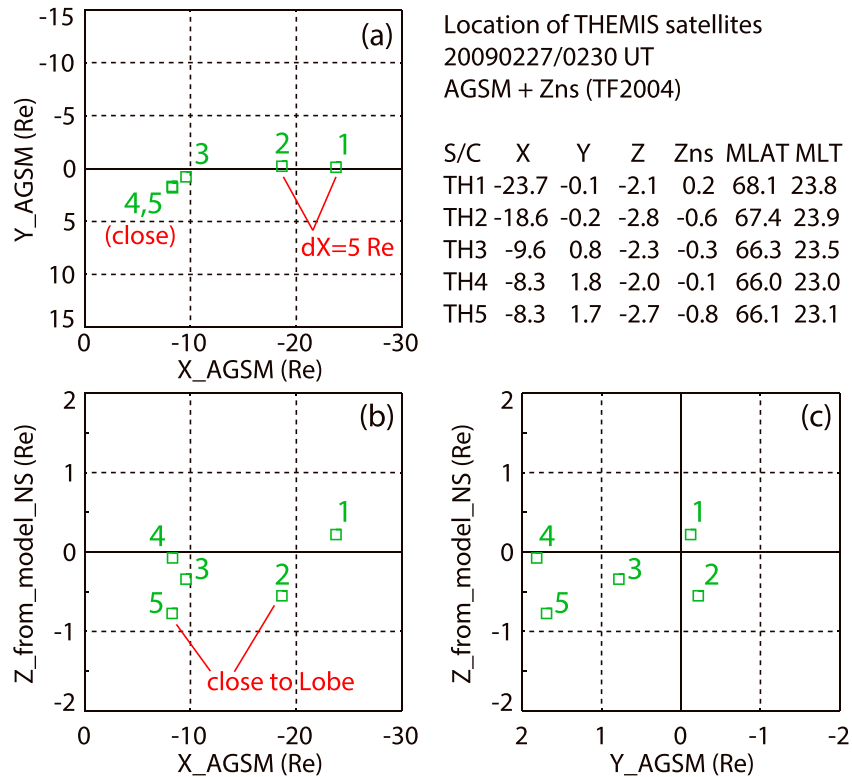


Figure 1. Locations of five THEMIS satellites at 0230 UT on 27 February 2009. Projected on (a) XY, (b) XZ, and (c) YZ planes in aberrated geocentric solar magnetospheric (AGSM) coordinates. The Z location in Figures 1b and 1c is the distance from a model neutral sheet instead of that from the equatorial plane. Magnetic latitude (MLAT) and magnetic local time (MLT) are satellite foot points at 110 km altitude in the modified apex coordinates.

[Iyemori, 1990], obtained from the Operating Missions as Nodes on the Internet (OMNI) [King and Papitashvili, 2005] 1 min data. We used SYM-H instead of the Dst index (1 h resolution) because of its superior time resolution. We used these parameters after calculating 1 h backward running averages from 60 min before the time of interest.

2.3. All-Sky Imager and Ground Magnetometer

Ionospheric signatures were obtained by the THEMIS Ground-Based Observatories (GBO) [Mende et al., 2008]. GBO consists of about 20 white-light all-sky imagers (3 s resolution) [Donovan et al., 2006] and magnetometers (0.5 s resolution) [Russell et al., 2008] deployed near the auroral zone of the North American continent and Greenland. We also used magnetometers operated by the Technical University of Denmark (DTU), Canadian Array for Realtime Investigations of Magnetic Activity (CARISMA), Magnetometer Array for Cusp and Cleft Studies (MACCS), Geophysical Survey of Canada (GSC), and the United States Geological Survey (USGS).

We used two ground stations imagers: Narsarsuaq (NRSQ, 65.4 MLAT, 61.2°N, 314.6°E) in southern Greenland and Sanikiluaq (SNKQ, 66.1 MLAT, 56.5°N, 280.8°E) in eastern Canada (Figure 2). Auroral images from Kuujuaq (KUJJ) in eastern Canada were not used owing to cloud cover.

3. Observations

3.1. All-Sky Images and Keogram

Figures 3 and 4 show five auroral brightenings, which started at 0213:36, 0219:36, 0225:00, 0237:21, and 0245:21 UT. Brightenings were visually identified using the original 3 s resolution images, with subjective accuracy to approximately 9–15 s.

3.1.1. Precursory Brightening and Akasofu Initial Brightening

The first brightening was initiated at 0213:36 UT at [23.5 MLT, 66.0 MLAT] (Figures 3a and 4c) but at this point was faint and difficult to identify without comparison with other images. Subsequently, the brightening expanded westward and spanned between 23.0 and 23.6 MLT 2 min later (Figure 3b), when auroras were

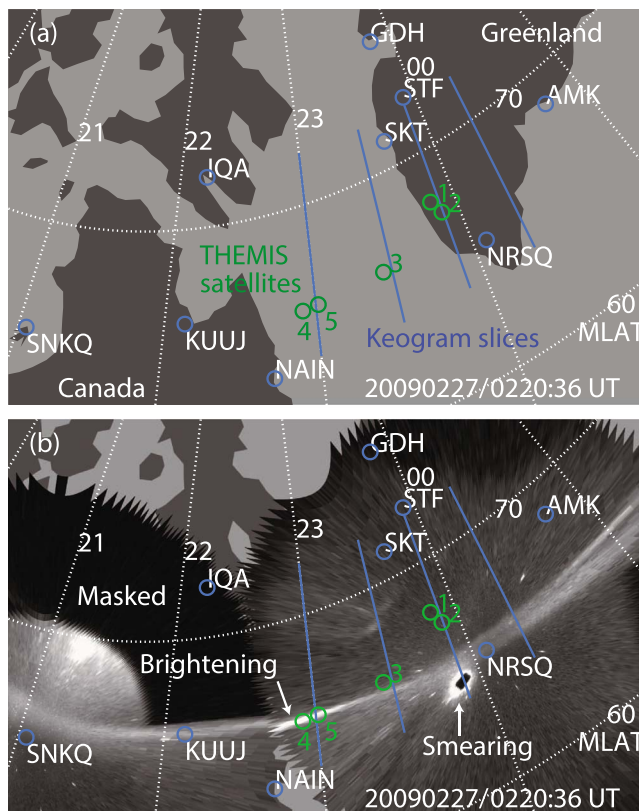


Figure 2. Ground observatories, satellite foot points, and an example merged auroral image. (a) Locations of ground observatories in southern Greenland and eastern Canada, as shown by blue circles with white labels. Some observatories were located outside of the latitude range of this figure. White lines with labels indicate magnetic latitude (MLAT) and magnetic local time (MLT). Green circles with numbers indicate satellite foot points of the five THEMIS satellites. The four blue lines (at 23.0, 23.5, 23.9, and 0.3 MLT) indicate the locations where images were sliced to make auroral keograms (Figure 4). (b) An example of merged auroral images overlaid to Figure 2a. Images were observed at Narsarsuaq (NRSQ, 65.4 MLAT, 61.2°N, 314.6°E) in Greenland and at Sanikiluaq (SNKQ, 66.1 MLAT, 56.5°N, 280.8°E) in Canada. The fan-like black area in the SNKQ image was masked to avoid artificial light.

at their brightest. Since this brightening was relatively weak and subsequently faded (Figure 3c) within a few minutes, we classified it as a precursory brightening.

The second brightening, which was initiated at 0219:36 UT (6 min after the first brightening) at [23.0 MLT, 66.0 MLAT] (Figures 3d and 4d), quickly expanded longitudinally, spanning approximately 22.6–23.4 MLT 1 min later (Figure 3e), and approximately 21.9–23.4 MLT 2 min later (Figure 3f). Since this brightening occurred nearly simultaneously (within a few minutes) across a wide longitude, we interpreted it to be the “initial brightening,” used to define the substorm onset by Akasofu [1964].

Akasofu [1964] showed that a substorm expansion phase onset is defined by two stages: a sudden brightening wide in longitude (0–5 min after onset) and poleward expansion (5–10 min after onset). This sudden brightening (substorm onset in Akasofu [1964]) is traditionally referred to as the initial brightening; however, it is not necessarily the first observed brightening in an event. We refer to this initial brightening as the Akasofu initial brightening to avoid confusion with the first brightening.

Such wide brightening may exhibit bead-like longitudinally separated structures; however, in this case these were not clear, possibly because the camera line-of-sight directions to the brightening were parallel to the brightening arc. Alternatively, auroral beads may not always be included in the Akasofu initial brightening.

3.1.2. Auroral Breakups

The third brightening occurred at 0225:00 UT (Figures 3h and 4c), 5 min after the second brightening. This brightening was initiated at [23.5 MLT, 65.9 MLAT], and the area west of this MLT brightened almost simultaneously (e.g., 23.0 MLT) within the period of uncertainty for the identifications (~9–15 s). The aurora also expanded poleward (Figures 3i–3k); thus, this brightening was classified as an auroral breakup.

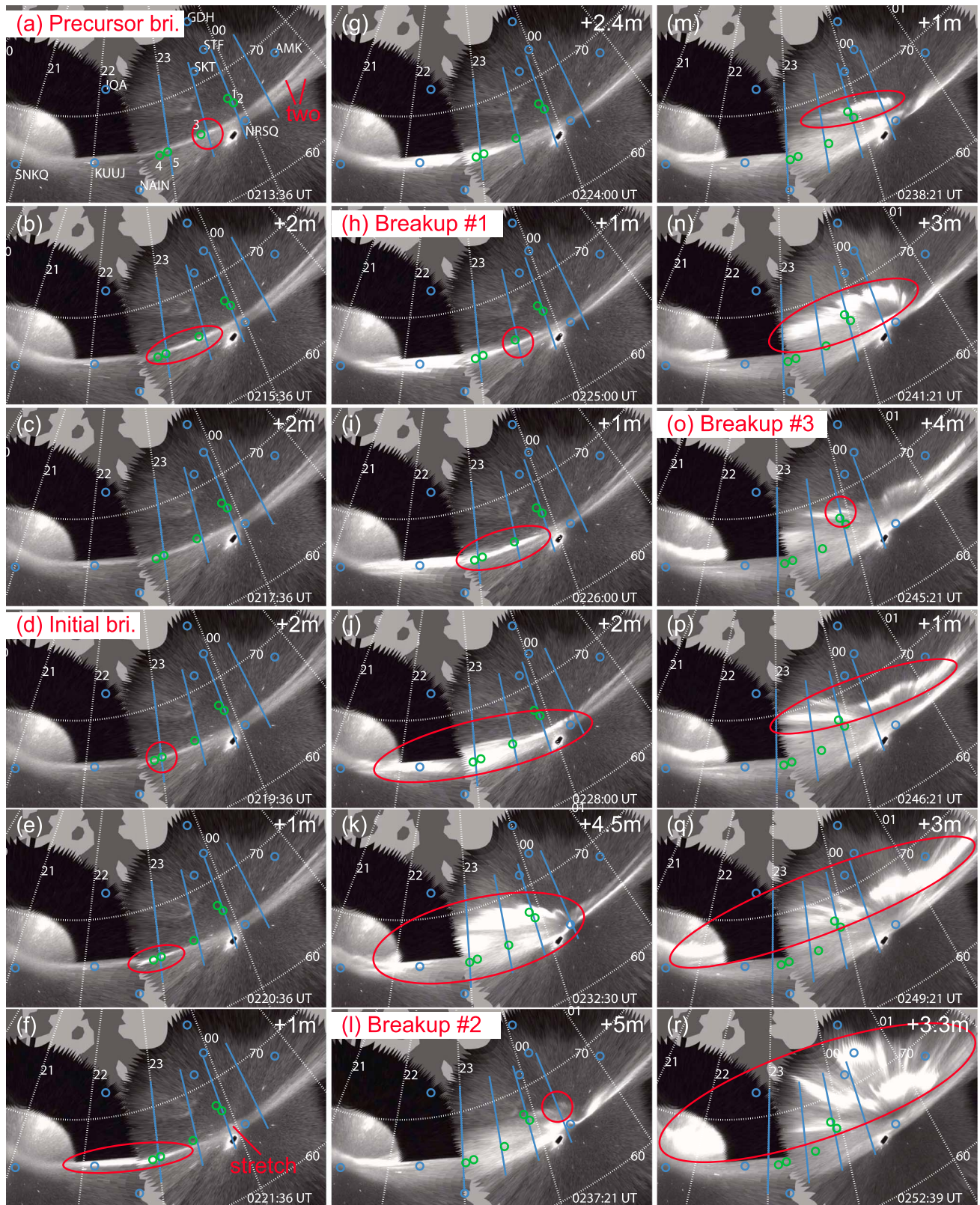


Figure 3. Time sequence of selected white-light auroral images on 27 February 2009. The five auroral brightenings are classified as (a) precursory brightening, (d) Akasofu initial brightening, and (h,l,o) auroral breakups, as labeled on the top left of corresponding panels. Images are typically separated by 1–2 min (but up to 5 min), as shown at the top right of each panel. More explanation of a panel can be found in the caption of Figure 2.

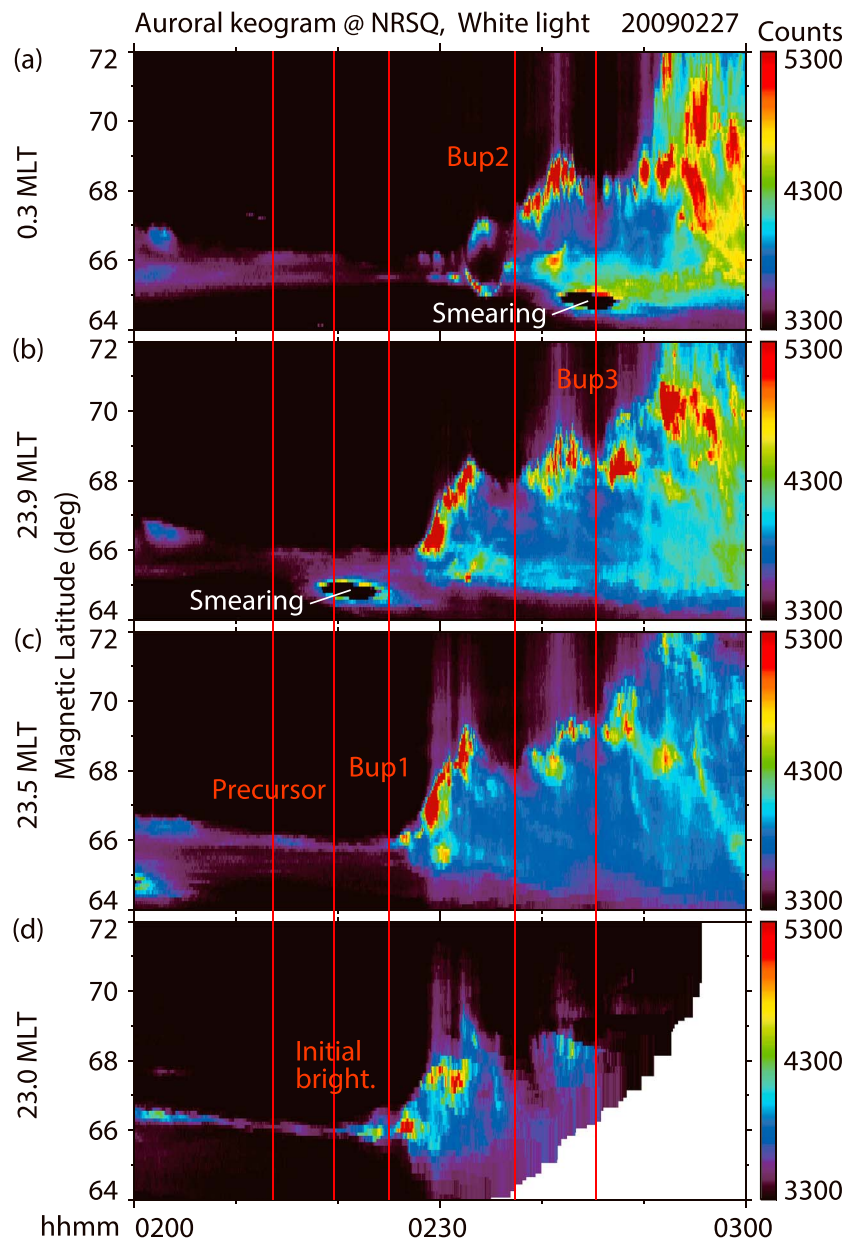


Figure 4. Auroral keograms sliced at (a) 0.3, (b) 23.9, (c) 23.5, and (d) 23.0 MLTs, corresponding to four blue lines placed from east to west in Figures 2 and 3. The red vertical lines indicate the times of five auroral brightenings, which were identified in the original sequence of images. Labels indicate the precursory brightening, the Akasofu initial brightening, and auroral breakups, as shown in the panel that corresponds to the magnetic local time (MLT) where each brightening was first recognized.

The poleward edge of the auroras expanded poleward to 69.3 MLAT and subsequently returned to 68.5 MLAT, where they faded at 0236:00 UT (Figure 4c).

The fourth brightening occurred at 0237:21 UT (Figures 3l and 4a), 12 min after the previous brightening. It was initiated at [0.3 MLT, 67.2 MLAT] and rapidly expanded westward to reach TH3 (23.5 MLT) within 1 min (Figure 3m). This brightening also expanded poleward (Figure 3n); thus, it was also classified as a breakup in this study. During the westward expansion of this brightening, corresponding brightenings were observed locally at 68.1 MLAT at 23.9 MLT (Figure 4b), and at 68.5 MLAT at 23.5 MLT (Figure 4c) within 1 min. These three initiation latitudes were within $\sim 0.2^\circ$ of the end-time latitude of poleward edge of the previous breakup (Figures 4a–4c) and were 1.1–2.6° higher than the start-time latitude of the previous breakup, depending on the MLTs.

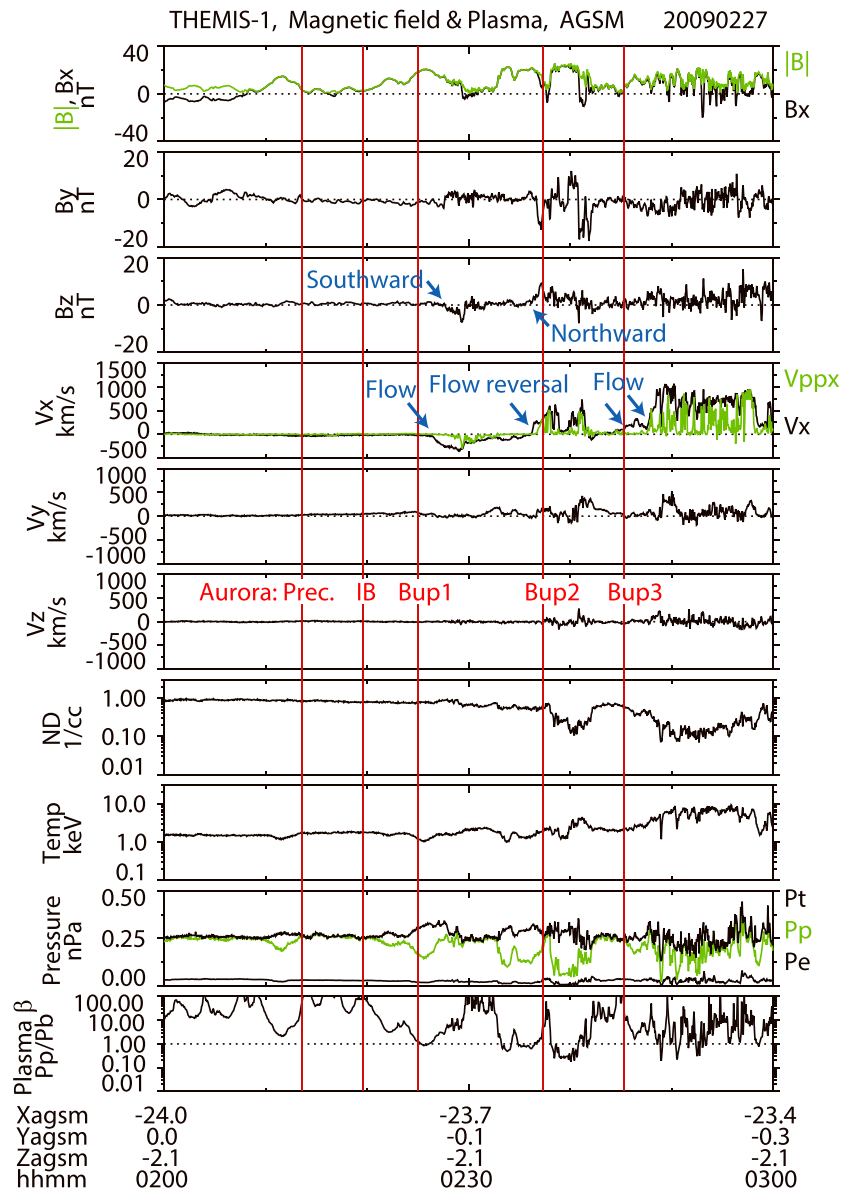


Figure 5. Time History of Events and Macroscale Interaction during Substorms probe 1 (THEMIS 1) satellite observations of the magnetotail with a 3 s time resolution. The red vertical lines indicate the times of auroral brightenings. The top three panels show magnetic field data, while the next five panels show ion velocities, density, and temperature. V_{ppx} indicates the X component of the velocity perpendicular to the magnetic field. In the next panel pressures are superposed, including the static total pressure (magnetic pressure plus plasma thermal pressure), the plasma thermal pressure, and the electron thermal pressure. The bottom panel shows the plasma beta (ratio of the plasma thermal pressure to the magnetic pressure). Electrostatic analyzer (ESA) ion and electron data and solid state telescope (SST) ion data are included, but SST electron data are not included.

The fifth brightening occurred at 0245:21 UT (Figures 3o and 4b), 8 min after the previous one. This brightening was initiated at about [23.9 MLT, 68.5 MLAT], but also spanned a wide range of longitudes, at least 23.2–1.5 MLT within 1 min (Figure 3p), starting at 68.0 MLAT at 0.3 MLT (Figure 4a), and at 69.1 MLAT at 23.5 MLT (Figure 4b). These brightenings also expanded poleward (Figures 3q and 3r) and thus were considered to represent breakup in this study. This third breakup started within ~ 0.1 degrees of the end-time latitude of the poleward edge of the previous breakup, and was 0.4–0.8 degrees higher than the start-time latitude of the previous breakup, depending on MLTs. This third breakup included an auroral activation at 72 MLAT (Figure 3r), which was presumably close to the polar cap boundary.

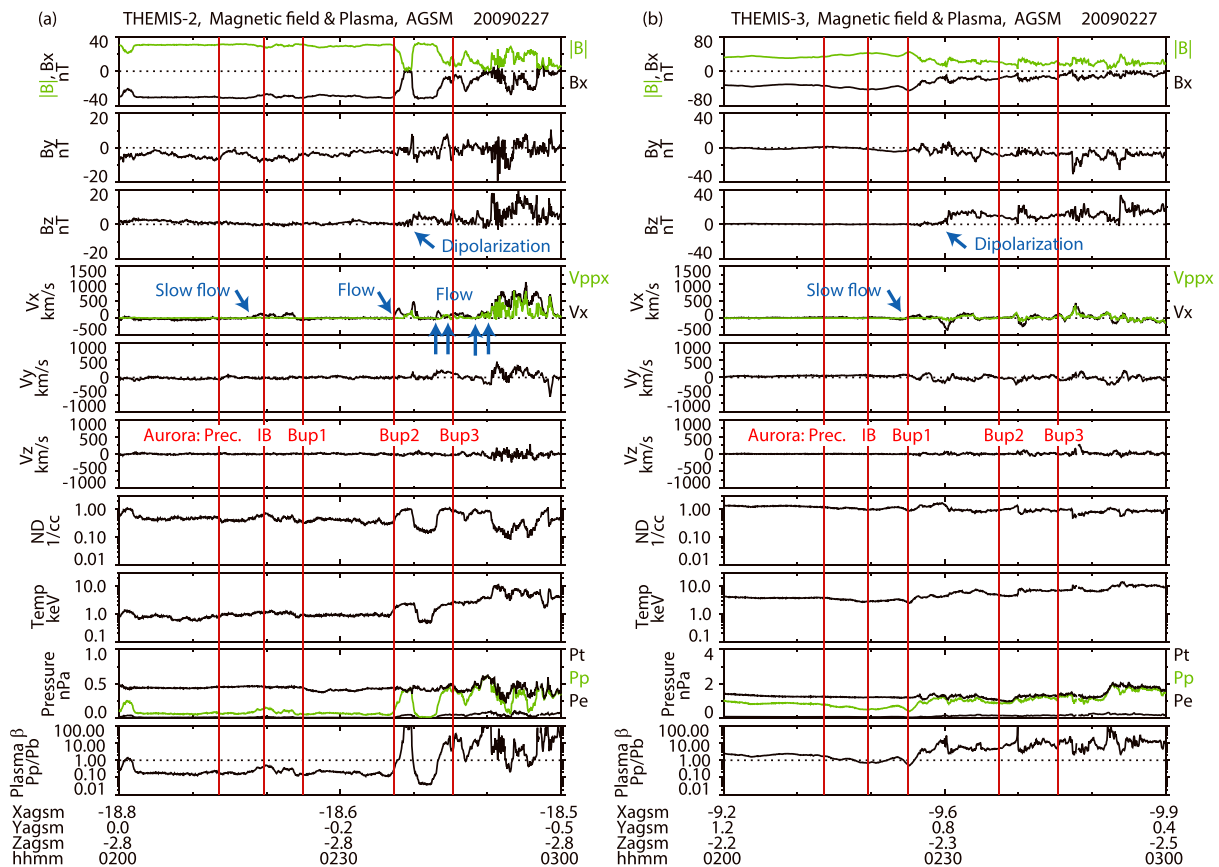


Figure 6. (left) THEMIS 2 and (right) THEMIS 3 satellite observations of the magnetotail in the same format as Figure 5.

In summary, auroral breakups repeated at approximately 10 min intervals. The next breakup tended to occur near the end-time poleward edge of the previous breakup. In other words, later breakups were initiated at higher latitudes; that is, auroral breakups occurred stepwise.

3.2. THEMIS Satellite Observations

Figures 5–9 show THEMIS satellite observations of the magnetotail. In summary, the THEMIS satellite observations showed that the tail reconnections did not correspond to the Akasofu initial brightening but to the auroral breakups. A flow reversal was observed at the second breakup before the third breakup, indicating that the tailward retreat of the neutral line was initiated during the substorm expansion phase.

All five THEMIS satellites typically stayed within the plasma sheet, since the plasma beta was typically greater than 0.1 for all satellites, including TH1 (Figure 5), TH2 (Figure 6a), TH3 (Figure 6b), TH4 (Figure 7a), and TH5 (Figure 7b). TH1 and TH4 tended to remain located in the central plasma sheet (CPS), deep within the plasma sheet, while TH2 and TH5 were often located at the plasma sheet boundary layer (PSBL), close to the tail lobe.

3.2.1. Precursory Brightening (0213:36 UT, 23.5 MLT)

At the initiation of the precursory brightening, no fast flow was observed by the five THEMIS satellites (Figure 8a). TH5 (Figure 7b, 23.0 MLT, $X = -8 R_E$) was located near the lobe and observed a quasiperiodic (~ 3 min) oscillation in the magnetic field, predominantly in the Y component, with an amplitude of about 2 nT. This magnetic oscillation started at 0213 UT and continued for at least three cycles until 0225 UT, when the first breakup was initiated. The plasma flow also oscillated predominantly in the Y component with an amplitude of 20 km/s (too low to see in Figure 7b).

Magnetic oscillations in the tail are sometimes suggested to manifest as ballooning mode instability in association with substorm onset [Cheng and Lui, 1998; Saito et al., 2008]. The magnetic oscillations in the tail (Figure 7b) were accompanied by the precursory brightening at 0213:36 UT; thus, the start of magnetic oscillations does not necessarily mark a substorm onset.

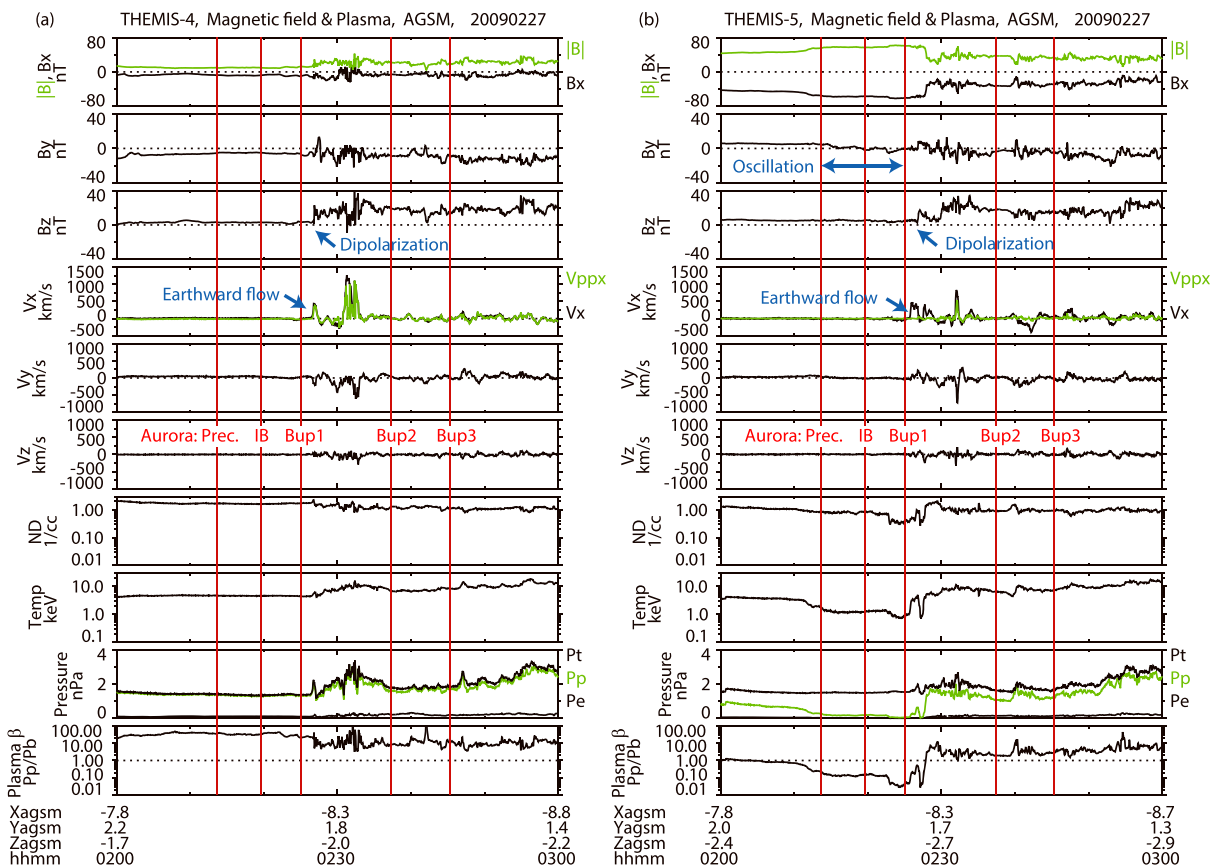


Figure 7. (left) THEMIS-4 and (right) THEMIS-5 satellite observations of the magnetotail in the same format as Figure 5.

3.2.2. Akasofu Initial Brightening (0219:36 UT, 23.0 MLT)

The longitudes of the second brightening (i.e., “Akasofu initial brightening”) were close to the foot points of TH4 (22.9 MLT) and TH5 (23.0 MLT). However, neither satellite, located at $X = -8.2 R_E$, observed significant flows or dipolarizations (Figure 8). In particular, TH4 observed no plasma flow, although TH4 was located deep inside the CPS, as seen in the high (>10) plasma beta (Figure 7a). In addition, no flow was observed at the TH3 location (23.4 MLT, $X = -9.6 R_E$) either. Therefore, it is likely that no convective earthward fast flows occurred in the plasma sheet near the Akasofu initial brightening (23.0 MLT).

TH2 (Figure 6a, 23.9 MLT, $X = -19 R_E$) and TH1 (Figure 5, 23.8 MLT, $X = -24 R_E$) were located ~ 0.5 MLT hours east from the eastern edge of the Akasofu initial brightening (21.9–23.4 MLT), thus, making it marginally possible for these two satellites to detect possible flows because the flow center is typically displaced 0.4 h east from the brightening [Nakamura *et al.*, 2001]. TH2 was located in the PSBL and observed an earthward flow at about 0218:08 UT, 1.5 min before the Akasofu initial brightening. However, this precursor earthward flow was slow (peak $V_x = 133$ km/s) and was parallel to the magnetic field. Moreover, TH1 observed no flows, despite being located deep within the CPS. Therefore, it is likely that the slow earthward flow observed by TH2 was not associated with developed NENL or with the distant neutral line.

The implication of the slow precursor earthward flow at $X = -19 R_E$ is unknown, but a statistical study also suggested earthward flows in the plasma sheet inside $20 R_E$ down the tail, occurring a few minutes prior to tailward flows farther down the tail [Machida *et al.*, 2014]. These precursor earthward flows may be associated with the initial stage of reconnection. A stage of weak reconnection is expected prior to its major development [e.g., Nishida *et al.*, 1986; Russell, 2000; Pu *et al.*, 2010]. Alternatively, the precursor earthward flow may have been associated with possible localized plasma loss and resultant plasma sheet thinning farther down the tail. An enhancement in V_y from 20 km/s (0213 UT) to 90 km/s (0225 UT) observed by TH1 ($X = -24 R_E$) may indicate an enhancement of the diamagnetic current caused by the thinning. A precursor earthward flow

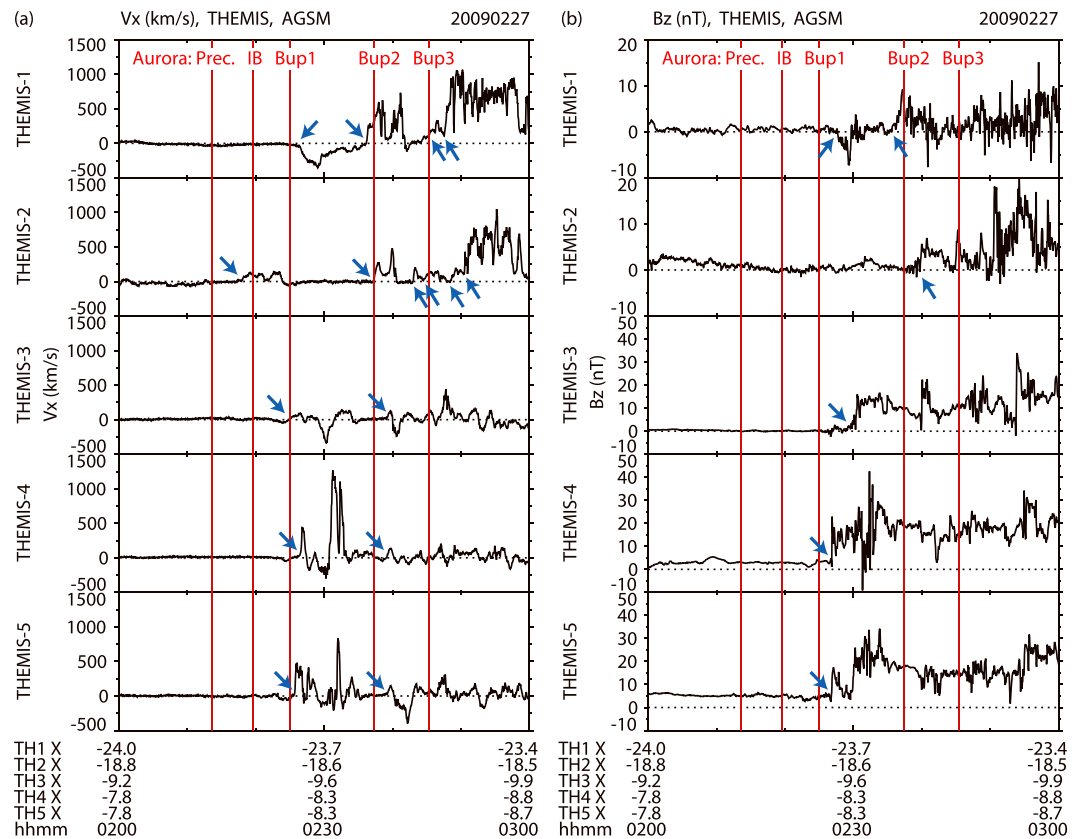


Figure 8. Observations by five THEMIS satellites: (a) the earthward component of ion flow velocity (V_x) and (b) the northward component of magnetic field (B_z). These parameters are the same as those shown in Figures 5–7 for each satellite. The red vertical lines indicate the times of auroral brightenings. Blue arrows indicate the times of characteristic signatures. Data from the electrostatic analyzer (ESA) and solid state telescope (SST) instruments were merged to calculate ion velocity.

is suggested to be associated with plasma sheet thinning just prior to a major reconnection also in kinetic simulations [Sitnov et al., 2014; Liu et al., 2014].

Three enhancements in the earthward going ions were observed by the ESA instrument on TH2 (Figure 9a). The second enhancement occurred just before the Akasofu initial brightening and corresponded to the slow earthward flow at about 0218:08 UT, where tailward going ions lowered the flow speed in the velocity moment. The first enhancement may be associated with the precursory brightening; although corresponding enhancement was barely visible in V_x (Figures 6a and 8). Thus, precursor brightenings may be associated with plasma transportation even when plasma flow is not evident in the velocity moments. In summary, reconnection was not developed or quite localized around the times of the Akasofu initial brightening.

3.2.3. First Breakup (0225:00 UT, 23.5 MLT)

TH1 ($X = -24 R_E$) observed a tailward flow at 0226:27 UT at 23.9 MLT, followed by a southward magnetic field (Figure 5). These signatures indicated that a reconnection occurred on the earthward side of TH1 within a few minutes of the first breakup. Since V_y decreased slightly during the tailward flow, TH1 was likely located somewhat dawnside of the reconnection center [Ieda et al., 1998].

At about the same time, TH4 (0226:25 UT, 23.0 MLT) and TH5 (0225:42 UT, 23.1 MLT) observed fast (>300 km/s) earthward flows that support this reconnection at the first breakup. TH4 and TH5 further observed dipolarization at about 0226:50 UT. A few minutes later, very fast earthward flow (1200 km/s) was observed by TH4 (start: 0230:46 UT, peak: 1300 km/s at 0231:16 UT) and TH5 (start: 0231:52 UT, peak 830 km/s at 0232:01 UT). These later flows were simultaneous with a further auroral activation at 0231 UT near 68.2 MLAT (Figure 4c).

TH3 also observed earthward flow at about 0225:00 UT; however, the flow (95 km/s at peak) was slower and less clear than would be expected given the nominal closeness of TH3 (23.5 MLT) to the breakup location

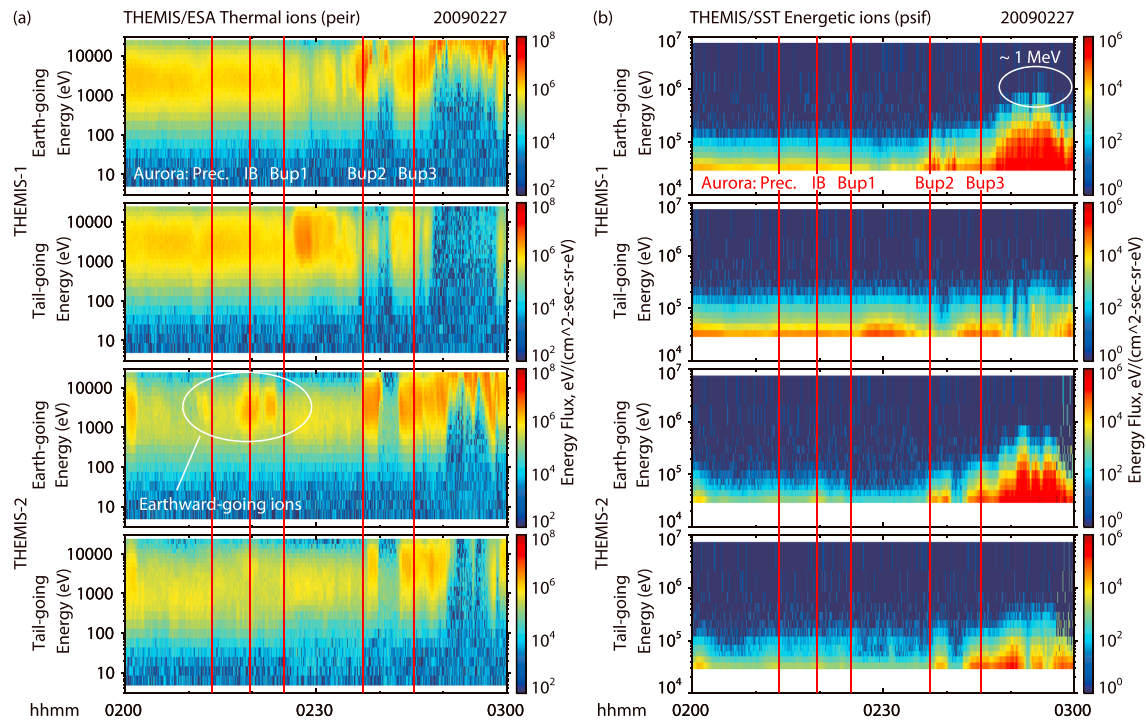


Figure 9. Ion energy flux observed by two THEMIS satellites. (a) Electrostatic analyzer (ESA) observations between 5 and 25 keV. (b) Solid state telescope (SST) observations between 25 keV and 6 MeV. The top two panels show THEMIS probe 1 observations of earthward going and tailward going ions. The bottom two panels show THEMIS probe 2 observations in the same format. The earthward going direction was defined as inside 45° from the X direction in the satellite coordinates, which was close to the direction to the Earth. The tailward going direction was defined as the opposite.

(23.5 MLT). TH3 subsequently observed a tailward flow with a dipolarization at 0229:11 UT. This tailward flow would be a return flow of a possible earthward flow with its center somewhat duskside of the TH3 location.

TH2 did not observe flows, presumably because it was located near the tail lobe, but it did observe a decrease in the total pressure, beginning around 0224:58 UT, suggesting that it was located near the reconnection XY location [Miyashita et al., 2009]. In summary, the first breakup was consistent with the formation of a neutral line.

3.2.4. Second Breakup (0237:21 UT, 0.3 MLT)

TH1 (23.9 MLT) observed a reversal of flow direction from tailward to earthward at 0236:09 UT, with an enhancement of the northward magnetic field, corresponding to the second breakup (Figure 3). This flow reversal was consistent with the tailward motion of an NENL over a satellite (Figure 10). Tailward motion is classically supposed to start at the beginning of the recovery phase [Hones et al., 1973; Baumjohann et al., 1999].

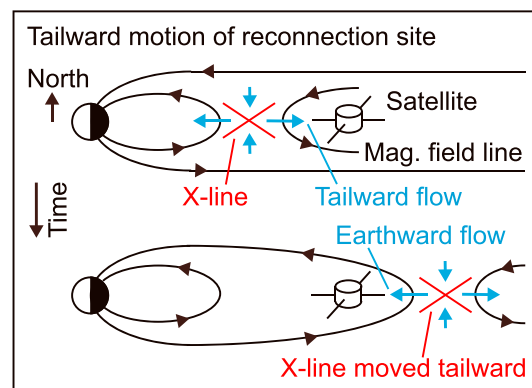


Figure 10. Inferred motion of the reconnection site, based on single satellite observations of the reversal of directions in the plasma flows and magnetic field.

In contrast, for this event the tailward motion started during the expansion phase. The flow reversal coincided with a breakup, suggesting that this flow reversal did not represent a quasi-static moving local spatial structure, but rather a global temporal change. In previous studies, the tailward motion of the NENL has been inferred to be approximately 1 R_E /min [Russell and McPherron, 1973; Baker et al., 2002; Imada et al., 2007; Nagai et al., 2011; Alexandrova et al., 2015]. In contrast, TH2 (23.9 MLT), which was located 5 R_E earthward of TH1, observed a similar earthward

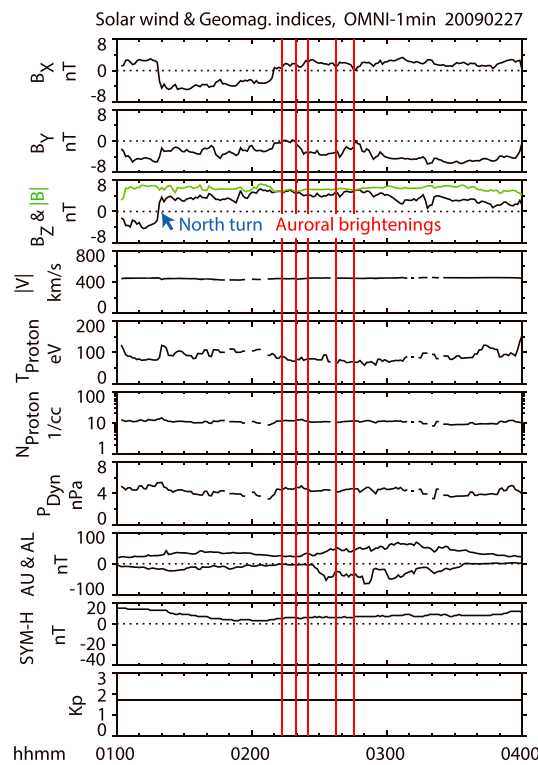


Figure 11. Operating Missions as Nodes on the Internet (OMNI) data set including solar wind parameters and geomagnetic indices. The red vertical lines indicate the times of auroral brightenings. The solar wind parameters are time shifted to the bow shock nose. Geocentric solar magnetospheric (GSM) coordinates were used. The interplanetary magnetic field (IMF) was mostly northward.

3.2.5. Third Breakup (0245:21 UT, 23.9 MLT)

TH1 (23.9 MLT) observed an earthward flow at 0245:18 UT, at approximately the time of the third breakup, suggesting that another reconnection was likely initiated. The earthward flow became further enhanced at 0247:35 UT, which may have been associated with the further poleward expansion beginning at approximately 0250:12 UT (Figure 4b) at least up to ~ 72 MLAT in a few min (Figure 4a). Since this latitude is presumably near the polar cap boundary, the third breakup with an earthward flow is consistent with the poleward leap phenomenon [Hones *et al.*, 1973].

TH2 (23.9 MLT) observed several earthward flows between 0243 and 0250 UT. Although it is difficult to conclude a one-to-one correspondence between the flows observed by TH2 and auroras, these flows appeared to be activated in association with the third breakup.

The flow oscillations observed by the TH3 (23.6 MLT), TH4 (23.1 MLT), and TH5 (23.2 MLT) satellites, which were initiated at the time of the second breakup, continued on a time scale of 2 min. Enhancements of earthward flow observed at around 0246:58 UT by TH3 may have been associated with the third breakup, but this conclusion remains speculative. In summary, the TH1 observation of an earthward flow indicated a new reconnection at the time of the third breakup, with the observations from other satellites not inconsistent with the new reconnection.

3.3. Solar Wind and Ground Magnetic Field

The north-south component of the interplanetary magnetic field (IMF) was northward from 0119 UT (about 1 h prior to the first brightening) to 0300 UT, with a mean value of 4 nT (Figure 11). The solar wind speed (about 440 km/s), plasma density (11 per cm^3), and dynamic pressure (4 nPa) were relatively high and stable during the 3 h period.

flow at 0237:08 UT, 1 min later than the TH1 observation. Since the earthward flow was observed nearly simultaneously (within 1 min) between the $5 R_E$ separated satellites, and even the inner satellite (TH2) observation was slightly later, this flow reversal is not likely to indicate the motion of a single X line but rather the creation of a new X line tailward of the TH1 location. TH2 observed a moderate dipolarization around 0239:45 UT, suggesting that the magnetic pileup front (outer edge of the dipolar field region) moved to around the TH2 location ($X = -19 R_E$), 4 min after the flow reversal at the TH1 location ($X = -24 R_E$).

TH3, TH4, and TH5 (at 23.5, 23.0, and 23.1 MLT, respectively) observed slow earthward flow at about 0239:15 UT, presumably corresponding to the arrival of westward expanding auroras. It is likely that these flows were slowed down inside the dipolarized region. These earthward flows were followed by tailward flows, which may indicate flow rebound. The flows oscillated on a time scale of 2 min at each of these three satellites. In summary, the NENL suddenly jumped tailward at the second breakup (i.e., during the expansion phase).

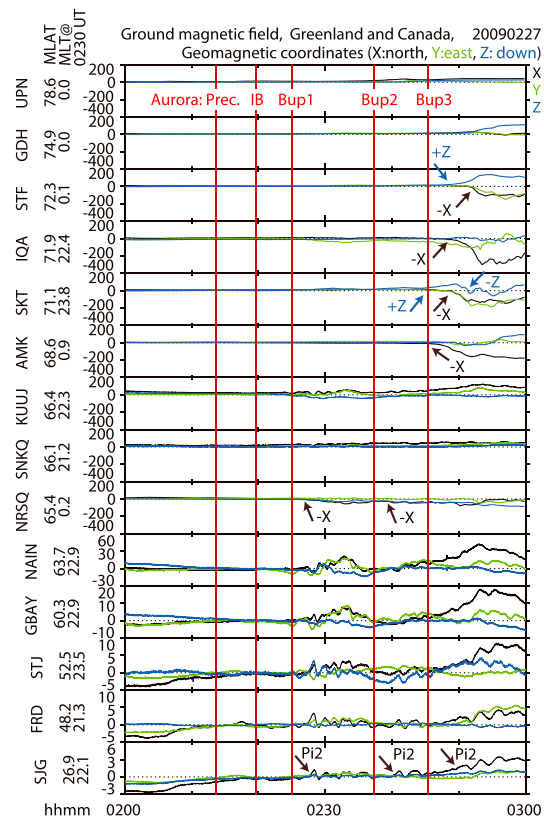


Figure 12. Ground magnetic observations near the longitudes of western Greenland and eastern Canada. Panels are presented in order of observatory latitude, with the top panel corresponding to the highest magnetic latitude (MLAT) station. The magnetic local time (MLT) of each observatory at 0230 UT is shown on the left of each panel. The locations of most stations are as shown in Figure 2. Variations in the northward (X), eastward (Y), and downward (Z) components of the magnetic field in geomagnetic coordinates. Data with latitudes of higher than 65 MLAT were subtracted using a five quiet-day baseline. Lower latitude data were subtracted by the median of the day.

At AMK (68.6 MLAT, 0.9 MLT), a negative X with negligible Z was detected, suggesting that the WEJ associated with the third breakup (which occurred at 0245:21 UT) started roughly around this latitude. At about the same time, a positive Z followed by a negative Z and then a negative Z was observed at station SKT (71.1 MLAT, 23.8 MLT), indicating that a WEJ was initiated at latitudes lower than SKT and then moved poleward over SKT. This poleward motion was consistent with observations of positive Z (0250 UT) and then negative X (0252 UT) at station STF (72.3 MLAT). This poleward shift over SKT and toward STF was also seen in the auroral images (Figures 3q and 3r). The results suggest that the WEJ center was initiated at approximately 69 MLAT and moved to approximately 71–72 MLAT, which is presumably close to the polar cap boundary. At station IQA (71.9 MLAT, 22.7 MLT), a negative X (0248 UT) was observed 2 min after the third breakup, followed by a peak X of -300 nT. This peak was the strongest observed among all observatories during this event, and station IQA probably detected a westward traveling surge. The observation of maximum WEJ at a relatively high latitude (71.9 MLAT) for a substorm during northward IMF is consistent with the results of Kamide and Akasofu [1974].

Pi2 range (40–150 s) magnetic pulsations were observed by a low-latitude (26.9 MLAT) station at San Juan (SJG) (Figure 12). The pulsations were not evident around the times of the precursory (0213:36 UT) and Akasofu initial brightenings (0219:36 UT); although, a weak pulsation could be identified at 0216 UT. In contrast, significant Pi2 pulsations were observed at 0228, 0240, and 0249 UT, a few minutes after each breakup. The amplitude (not shown) of these three major Pi2 pulsations were 0.5, 0.3, and 0.2 nT, respectively, in the wave index [Nosé *et al.*, 2012] at SJG (W_{SJG}), while the amplitude (not shown) was lower than 0.07 nT before 0225 UT. The second and the third ground pulsations appeared to be delayed by approximately 1 min after the plasma flow oscillations observed by TH3, TH4, and TH5 (Figure 8).

The AL index started to develop, albeit weakly, at 0228 UT (Figure 11), 3 min after the first breakup. The first peak reached -53 nT at 0233 UT, while the second peak reached -64 nT at 0250 UT. The SYM-H index [Iyemori, 1990] was positive, which is consistent with the high solar wind dynamic pressure.

Figure 12 shows variations in the northward (X), eastward (Y), and downward (Z) components of the ground magnetic field in geomagnetic coordinates. The precursory brightening (0213:36 UT) and the Akasofu initial brightening (0219:36 UT) occurred between KUUJ and NRSQ (Figure 3), but the corresponding magnetic bays were not evident in the ground-based magnetic observations from eastern Canada and southern Greenland (Figure 12). The first (0225:00 UT) and the second (0237:21 UT) breakups were accompanied by negative X (WEJ) at NRSQ, although the magnitude of the WEJ was weak (<100 nT). The bright auroral activity accompanying these breakups predominantly occurred in the latitude range between NRSQ (65.4 MLAT) and SKT (71.1 MLAT; Figure 3). In this region, magnetic bays were expected to be somewhat stronger; however, there was no geomagnetic observatory at this location and AMK was outside the eastern area of the active auroral area.

At AMK (68.6 MLAT, 0.9 MLT), a negative X with negligible Z was detected, suggesting that the WEJ associated with the third breakup (which occurred at 0245:21 UT) started roughly around this latitude. At about the same time, a positive Z followed by a negative Z and then a negative Z was observed at station SKT (71.1 MLAT, 23.8 MLT), indicating that a WEJ was initiated at latitudes lower than SKT and then moved poleward over SKT. This poleward motion was consistent with observations of positive Z (0250 UT) and then negative X (0252 UT) at station STF (72.3 MLAT). This poleward shift over SKT and toward STF was also seen in the auroral images (Figures 3q and 3r). The results suggest that the WEJ center was initiated at approximately 69 MLAT and moved to approximately 71–72 MLAT, which is presumably close to the polar cap boundary. At station IQA (71.9 MLAT, 22.7 MLT), a negative X (0248 UT) was observed 2 min after the third breakup, followed by a peak X of -300 nT. This peak was the strongest observed among all observatories during this event, and station IQA probably detected a westward traveling surge. The observation of maximum WEJ at a relatively high latitude (71.9 MLAT) for a substorm during northward IMF is consistent with the results of Kamide and Akasofu [1974].

Pi2 range (40–150 s) magnetic pulsations were observed by a low-latitude (26.9 MLAT) station at San Juan (SJG) (Figure 12). The pulsations were not evident around the times of the precursory (0213:36 UT) and Akasofu initial brightenings (0219:36 UT); although, a weak pulsation could be identified at 0216 UT. In contrast, significant Pi2 pulsations were observed at 0228, 0240, and 0249 UT, a few minutes after each breakup. The amplitude (not shown) of these three major Pi2 pulsations were 0.5, 0.3, and 0.2 nT, respectively, in the wave index [Nosé *et al.*, 2012] at SJG (W_{SJG}), while the amplitude (not shown) was lower than 0.07 nT before 0225 UT. The second and the third ground pulsations appeared to be delayed by approximately 1 min after the plasma flow oscillations observed by TH3, TH4, and TH5 (Figure 8).

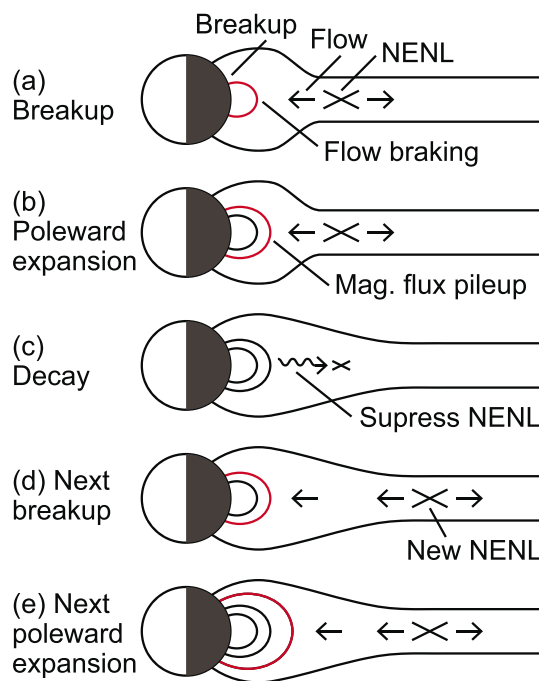


Figure 13. Interpretation of stepwise auroral poleward expansions. Time sequence of two successive auroral breakups is shown and the later breakup starts at a higher latitude: (a) Initiation of auroral breakup. Flow braking occurs on the magnetic field line on the dipole-tail boundary, as shown by the red curve. Auroral breakup occurs at the ionospheric foot point of this field line; (b) poleward expansion of auroras; (c) decay of auroras; (d) initiation of next auroral breakup; (e) next auroral poleward expansion.

ing tailward [Shiokawa et al., 1998]. The boundary location depends on the shape of the mapping field line [e.g., Chu et al., 2015] but should at least move tailward over a satellite that observes a dipolarization.

When a breakup decays (Figure 13c), the location of the dipole-tail boundary has been shifted tailward. If a reconnection is quickly reactivated (Figure 13d), a new flow braking occurs at this shifted location, so that the subsequent breakup is initiated at a latitude near the previous final latitude of the poleward edge of the bulge. Since this latitude is poleward of the latitude of the previous breakup onset, the breakup is observed as a poleward jump (i.e., the later breakup starts at a higher latitude).

4.1.2. Stepwise Jumps

Baumjohann et al. [1999] deduced that the tailward shift of the pileup front chokes the earthward outflow from the NENL. As a consequence, the NENL should move tailward due to the flux conservation requirement. They expected that the tailward retreat of the NENL starts when the piled-up front reaches the NENL location, because the NENL cannot operate in a dipolar field geometry. They used statistical methods to conclude that this tailward retreat starts approximately 45 min after the substorm onset, presumably at the beginning of the substorm recovery phase.

In contrast, the decay of the first breakup observed in this study suggests that the tailward shift of the pileup front may suppress earthward flow and the NENL during the expansion phase (Figure 13c). If the pileup region does not dissipate quickly, NENL should move away to a distant location (Figure 13d) in order to reactivate. This reactivation causes a repeat of the sequence, beginning with the next breakup (Figure 13d), followed by the next poleward expansion (Figure 13e).

In summary, we propose that magnetic pileup and the NENL interact during the expansion phase. In our scenario, multiple poleward expansions are associated with multiple reconnections through the multiple magnetic pileup. The model presented illustrates the case when the NENL reactivates quickly before the

4. Discussion

4.1. Interpretations of Stepwise Association

In this study, a tailward retreat was observed at the second breakup during the expansion phase. Since another tailward retreat was expected later at the beginning of the recovery phase [Hones et al., 1973], the NENL formation at the third breakup was probably associated with another tailward retreat. Thus, stepwise poleward expansion was likely associated with stepwise tailward retreat. We interpreted this relationship to be an indirect association, with both motions a consequence of the pileup of magnetic flux in the dipolar region (Figure 13).

4.1.1. Poleward Jump

The nightside magnetosphere generally has two regions: one with a dipole-like magnetic field geometry near the Earth, and the other with a stretched tail-like geometry. When a NENL is formed (Figure 13a), an earthward flow is ejected and brakes at the boundary between these two regions [Hesse and Birn, 1991; Shiokawa et al., 1997]. As the reconnection continues (Figure 13b), the earthward flow supplies the magnetic flux, which piles up at the dipole-tail boundary. This pileup corresponds to the auroral poleward expansion, forming an auroral bulge. The poleward edge of the expanding bulge is supposed to map back to the dipole-tail (pileup) boundary, which is shift-

piled-up magnetic flux dissipates (Figure 13). If the reactivation of NENL occurred relatively late, or piled-up magnetic flux dissipated quickly, breakups and NENL formation would instead repeat at nearly the same locations during the expansion phase.

4.2. Rediscovery of Poleward Leap and Update

Various auroral activations occur after a substorm onset. Among them, *Hones et al.* [1973] emphasized that activation near the polar cap boundary (PCB) at the beginning of the recovery phase (at auroral latitudes) is distinct and termed it the poleward leap. One objection to the poleward leap has been that there is no physical difference between such an activation and preceding activations [e.g., *Rostoker, 1986*]. However, phenomena similar to the poleward leap were independently reported as follows.

Anger and Murphree [1976] noticed that an auroral “bridge” forms when the auroral bulge joins an arc near PCB. Similar forms were called “double oval” by *Elphinstone et al.* [1993] and *Elphinstone et al.* [1995]. *Elphinstone et al.* [1996] stated that “the double oval forms when the aurora locally reaches its most poleward extent. At this time the aurora immediately equatorward within the bulge begins to fade.” This explanation of the double oval formation is essentially the same as the definition of the poleward leap phenomenon as “declining auroral zone currents, growing polar cap currents, and a thickening plasma sheet” [*Hones, 1986*]. Therefore, we believe that the double oval formation and the poleward leap are the same phenomenon. In contrast, *Elphinstone et al.* [1996] rejected the poleward leap concept because they did not find motions of auroras in their event, but they have not explained the reason why motions are expected for the poleward leap. We guess from their context that they interpreted the poleward leap concept as implying continuous poleward auroral motions, but such continuous motion is not specifically required in the poleward leap concept [e.g., *Hones et al., 1973; Hones, 1986*]. We believe that the emergence of new aurora at a higher latitude in the *Elphinstone et al.* [1996] event does not reject but rather supports the poleward leap concept.

In addition, some substorm activations in previous studies [e.g., *Milan et al., 2006; Nakamura et al., 2011; Cao et al., 2012*] are likely to represent the poleward leap phenomenon. Since rediscovered, the poleward leap is likely distinct from preceding auroral activations. Furthermore, the activation near the PCB sometimes occurs when the expanding aurora contacts an arc along the PCB [e.g., *Kadokura et al., 2002; Lyons et al., 2013*]. This contact suggests an interaction between the higher-latitude and lower latitude arc systems, which may explain why the poleward leap is different from the preceding activations.

Since the poleward leap is revealed to be distinct, the classical NENL model predicts two auroral poleward expansions (and one tailward retreat). In contrast, more than two auroral activations are often evident [*Kisabeth and Rostoker, 1974; Wiens and Rostoker, 1975; Pytte et al., 1976a; Rostoker et al., 1980*]. Another objection to the poleward leap phenomenon is that these total numbers do not match [e.g., *Rostoker, 1986*]. However, tailward retreat is not necessarily the equatorial counterpart of the originally proposed one-time auroral poleward leap at the beginning of the recovery phase, but can be a stepwise phenomenon too, one that is initiated during the expansion phase, as shown in this study. In other words, we are hereby updating the poleward leap concept to allow stepwise tailward retreat in order to explain the observed stepwise poleward expansion.

4.3. IMF Dependence and Periodic Formation of NENL

Angelopoulos et al. [1996] suggested that the NENL moved tailward during the expansion phase, based on a multiple plasmoid event observed by the Geotail satellite at $61 R_E$ down the tail. Successive plasmoids indicate successive formation of NENLs. They compared the duration of the leading and trailing parts inside plasmoids and noticed that later plasmoids tended to have shorter durations in the leading part (northward B_z). Such plasmoids were interpreted to be created by the NENL, relatively close to the satellite. Based on this interpretation, they concluded that later NENLs formed at successively more tailward locations that were closer to Geotail. This tailward motion was confirmed by multisatellite observations [*Angelopoulos et al., 2013*]. In the present study, we found that such tailward motion of the NENL was associated with stepwise auroral expansion.

In contrast, classically, the NENL does not move significantly during the substorm expansion phase [*Nishida and Nagayama, 1973*]. This is the case even for multiple-onset substorms as follows. *Ieda et al.* [2001] studied the association between plasmoid ejection and auroral brightening. Plasmoids were often observed repeatedly on a time scale of 10 min. Since they came from the earthward side, the NENL should have stayed earthward of the Geotail and within $30R_E$ down the tail. Thus, formation of a neutral line can repeat without

significant tailward retreat. Pytte *et al.* [1976a] investigated NENL locations during multiple-onset substorms. Locations were inferred from plasma sheet thinning and thickening, as observed by two satellites (Vela 4A at $18 R_E$ down the tail and Ogo 5 between 10 and $17 R_E$). They found that the NENL remained between the two satellites; thus, it did not move significantly during the expansion phase, even with multiple onsets.

Thus, NENL either moves tailward or stays during the expansion phase, presumably depending on background conditions. The cause of the classic tailward retreat at the beginning of the recovery phase is not well understood [e.g., Oka *et al.*, 2011], but it may be a consequence of the excess reconnection rate in the NENL, as compared with that in the dayside [Russell and McPherron, 1973; McPherron, 1991]. Thus, IMF B_z is expected to be associated with the tailward retreat.

In the present event, IMF was northward. During northward IMF, dayside reconnection and the return convection toward the dayside region are suppressed; thus, nightside piled-up magnetic field lines tend to be maintained. This may be the reason why the stepwise characteristics of the poleward expansion and tailward retreat were pronounced in the present event.

During southward IMF, piled-up magnetic flux dissipates and convects to the dayside. Thus, expanded auroras return to lower latitudes [Pytte *et al.*, 1976b], at least to some extent. Even in such circumstances, interactions between the piled-up region and the NENL (similar to that in Figure 13) may be also possible, but new auroral activation and NENL formation could repeat at nearly the same location. Since IMF is often southward during the initial stage of substorms, NENL may appear to stay during the expansion phase in a statistical sense.

Plasmoids are often observed quasiperiodically within a time scale of 10 min [Slavin *et al.*, 1993, 2002; Ieda *et al.*, 2001]. This periodicity suggests a quasiperiodic formation of the NENL, presumably as a consequence of the interaction between the pileup region and NENL, regardless of the IMF B_z polarity. An alternative interpretation of periodic plasmoids is simultaneous reconnection at multiple X lines [Slavin *et al.*, 2003] associated with tearing instability [e.g., Drake *et al.*, 2006].

4.4. Same or New NENL

A satellite observation of a sequence of tailward then earthward flow is often interpreted as the passage of a single NENL near satellites [e.g., Ueno *et al.*, 1999, 2003; Nagai *et al.*, 2005]. Eastwood *et al.* [2010] identified possible passages of the NENL using four Cluster satellites within $20 R_E$ down the tail. They identified 16 correlated field and flow reversal events. Using the time delay in the B_z profile, they confirmed that most (15 of 16) events were actually tailward passages of a single X -type neutral line, although the remaining event was interpreted to indicate the existence of two X lines [Eastwood *et al.*, 2005].

In contrast, Angelopoulos *et al.* [1996] suggested that flow reversal may indicate the creation of a new NENL. They further inferred that multiple reconnection sites can coexist simultaneously, based on observations of counterstreaming energetic particles at $61 R_E$ down the tail.

In the present study, TH1 ($X = -24 R_E$) observed a flow reversal at the second breakup. TH2 was located $5 R_E$ earthward of TH1 and observed an earthward flow 1 min later. These observations suggest that flow reversal does not indicate the motion of a single X line, but in reality the creation of a new NENL. However, the delay may be explained by the fact that TH2 was located closer to the tail lobe than TH1. Thus, the creation of a new NENL is suggested by the results of this study, but cannot be fully confirmed. It remains unclear whether flow reversals (i.e., tailward retreat) beyond $20 R_E$ down the tail actually represent smooth tailward motion of a single X line, or the creation of new reconnection sites. It may also be possible that new NENL are not strictly new, but rather are intensifications of old single NENL after tailward relocation.

4.5. Full Substorms

In the present case, the third breakup was accompanied by an auroral activation (Figure 3r) and a WEJ (Figure 12) near the nominal PCB latitude, a reconnection earthward flow (Figure 5), and energetic ions (Figure 9b). These signatures are consistent with the poleward leap phenomenon [Hones *et al.*, 1973]. We suggest that the poleward leap represents full substorm development in terms of the involvement of open magnetic field lines in the ionosphere. Such full substorm development occurs well after the beginning of lobe field reconnection.

4.5.1. Last Closed Field Line Myth

Full substorms are often interpreted to be different from pseudosubstorms due to the inclusion of the lobe reconnection. This interpretation is partly correct because huge energy dissipation should include the lobe reconnection. It is sometimes further interpreted that the reconnection of the last closed field line marks the time of full substorm development [e.g., Russell and McPherron, 1973; Russell, 2000]. However, this interpretation is based on a two-dimensional view of the magnetic field lines and is not proven.

In contrast, there is evidence that the lobe reconnection is not a sufficient condition for full substorms. Ieda *et al.* [2001] identified the lobe reconnection by the existence of postplasmoid flow and the magnetic field. They showed a case in which the lobe reconnection did not correspond to a full-fledged breakup, but only to a spatially localized auroral brightening. Ohtani *et al.* [2002] identified a lobe reconnection with very fast tailward flow and reached a similar conclusion.

The last closed field line reconnection and plasmoid ejection are often supposed to occur when the auroral expansion reaches the PCB [e.g., Elphinstone *et al.*, 1996; Baker *et al.*, 1996]. However, plasmoid ejection almost always occurs within a few minutes of auroral breakup [Ieda *et al.*, 2001, 2008], likely earlier than the arrival of poleward expanding aurora at PCB. Note that the NENL is not necessarily visible in aurora. For example, breakup auroras do not directly map to the NENL at least at the beginning; thus, the arrival of a poleward expanding aurora at PCB does not necessarily correspond to the initiation of lobe reconnection, but rather occurs later. Note also that the auroral activation near PCB occurs at the time of poleward leap in the classic NENL model [Hones *et al.*, 1973; Hones, 1976], simultaneously with the classical tailward retreat at the beginning of the recovery phase (i.e., significantly later than plasmoid ejection).

Since we revealed the poleward leap phenomenon to be distinct from preceding auroral activations, we propose to define the full substorm as the special class of substorm with a poleward leap (i.e., the auroral poleward expansion into the polar cap). As discussed above, this full expansion occurs later than the last closed field line reconnection. Observations of auroras indicate the interaction of the bulge with an arc near the PCB and the formation of “bridge” (i.e., “double oval”) [Anger and Murphree, 1976; Elphinstone *et al.*, 1993]. Thus, it would be reasonable to conclude that lobe reconnection spreads in the dawn-dusk direction at this moment. When the pileup front moves close to NENL, earthward flow will be significantly blocked. To overcome the resultant suppression of reconnection, the NENL may move tailward significantly and spread in the dawn-dusk direction. These processes would be one possible understanding of the full substorm sequence.

4.5.2. Energetic Particles

Hones *et al.* [1973] noticed that energetic particles are observed predominantly at the time of poleward leap and later. Thus, we recognize that the full substorm includes observations of energetic particles. It is not concluded whether or not the reconnection in the vicinity of an X-type region is a strong ion accelerator [e.g., Birn *et al.*, 2012]. Baker *et al.* [1979] postulated that energetic (>0.3 MeV) protons were produced in the plasma sheet only at substorm onset because of large induced electric fields. They further concluded that energetic protons were observed during the recovery phase because of the expansion of the plasma sheet enveloping the observing spacecraft at $18 R_E$ down the tail.

In contrast, in the present study, TH1 ($X = -24 R_E$) stayed in the plasma sheet throughout and observed energetic ions up to ~ 1 MeV after the third breakup (Figure 9b). Therefore, these ions were likely accelerated not at the substorm onset but later at the poleward leap (third breakup). Since TH2 ($X = -19 R_E$) observed moderately similar ions, there appeared to be no further acceleration between 24 and $19 R_E$ down the tail. Therefore, these ions were likely accelerated relatively near the reconnection region.

Baker *et al.* [1979] found that energetic (>0.5 MeV) proton events at $18 R_E$ were mostly (95%) observed during the southward IMF interval and that no event corresponded to IMF $B_z > 2$ nT. Thus, the IMF condition ($B_z \sim 4$ nT) of the present energetic (~ 1 MeV) ion event was exceptional and the acceleration mechanism may be different from other energetic ion events.

The generation mechanism of the energetic ions in this particular event is unknown, but it may have been associated with the rapid fluctuations in the magnetic field [e.g., Artemyev *et al.*, 2014] after the third breakup (Figure 5). The particle acceleration may have also been associated with spatially multiple formations of the NENL. In this particular event, the NENL formed successively and there was the possibility of coexistence of multiple reconnection sites. Under such circumstances, a Fermi-type particle acceleration may be expected.

Acknowledgments

A.I. wishes to thank A. T. Aikio, S.-I. Akasofu, O. Amm, D. N. Baker, H. Hayakawa, T. Hori, M. Hoshino, S. Imada, Y. Kamide, S. Kokubun, K. Liou, A. Nishida, N. Nishitani, M. Nosé, M. Oka, I. Shinohara, K. Shiokawa, M. I. Sitnov, J. M. Weygand, and A. N. Willer for their valuable comments. We acknowledge NASA contract NAS5-02099 for use of data from the THEMIS Mission (<http://themis.ssl.berkeley.edu/>). Specifically, we thank C. W. Carlson and J. P. McFadden for use of ESA data; D. Larson and R. P. Lin for use of SST data; K.-H. Glassmeier, U. Auster, and W. Baumjohann for the use of FGM data provided under the lead of the Technical University of Braunschweig and with financial support through the German Ministry for Economy and Technology and the German Center for Aviation and Space (DLR) under contract 50 OC 0302; S. Mende and E. Donovan for use of the ASI data, the CSA for logistical support in fielding and data retrieval from the GBO stations, and NSF for support of GIMNAST through grant AGS-1004736; S. Mende and C. T. Russell for use of the UCLA ground magnetometer (GMAG) data and NSF for support through grant AGS-1004814; Erik Steinmetz, Augsburg College for use of the MACCS GMAG data; Tromsø Geophysical Observatory for use of the Greenland GMAG data; the Geological Survey of Canada for use of the CANMON GMAG data; USGS Geomagnetism Program for use of GMAG data; I. R. Mann, D. K. Milling, and the rest of the CARISMA team for use of GMAG data. CARISMA is operated by the University of Alberta, funded by the CSA. The OMNI data were obtained from the GSFC/SPDF OMNIWeb interface at <http://omniweb.gsfc.nasa.gov>. The *AL*, *AU*, and *SYM-H* indices were provided by the WDC for Geomagnetism, Kyoto. The wave index was obtained from the substorm swift search interface at <http://s-cubed.info/>. The code of the modified magnetic apex coordinates was received from the CEDAR database at NCAR, which is supported by NSF. This work was supported by JSPS KAKENHI grants 16K05568, 23540524, 26247082, and 15H05815. This work was also supported by JSPS ASINACTR grant G2602, by NASA grant NNX12AJ57G, by the Magnus Ehrnrooth foundation and by the GEMISIS project of ISEE in Nagoya University.

4.6. Connection of Auroral Arcs

It is unclear why two stages (the Akasofu IB and the breakup) often appear in substorm onset. For the event in this study, there were two arcs separated by approximately 1° in MLAT at $>\sim 0$ MLT, to the east of the onset MLT (Figure 3a). These arcs gradually formed from diffuse aurora after around 0212 UT (Figure 4a). On the poleward arc the precursory brightening occurred near 23.5 MLT at 0213:36 UT (Figures 3a and 3b). Later, at the time of the Akasofu initial brightening (0219:36 UT; Figure 3d), the onset arc ($<\sim 23.6$ MLT) was disconnected around 23.8 MLT from the poleward arc. Subsequently, the onset arc was connected to the equatorward arc, and the disconnected poleward arc stretched westward (Figure 3f). This stretching may have corresponded to the slow field-aligned earthward flow observed by TH2 (Figure 6a, 23.9 MLT, $X = -19 R_E$). The poleward arc was further stretched westward and was connected at 23.5 MLT to the onset arc (Figure 3h), when and where the first breakup was initiated. The onset arc remained connected to the poleward arc (Figures 3j and 3k) after the breakup.

In summary, the precursory brightening occurred on the poleward arc, then the Akasofu initial brightening arc was connected to the equatorward arc, and finally the breakup arc was connected to the poleward arc again. This sequence suggests that two arc systems were involved in the substorm onset and that the Akasofu IB and auroral breakup were not continuous but distinct; however, without data on additional events it is unclear whether this sequence is common.

5. Summary

In this study, we investigated a multiple-onset substorm in order to clarify stepwise poleward expansions. Five successive auroral brightenings were identified at about every 10 min in all-sky images. These brightenings included a precursory brightening, the Akasofu initial brightening, and three auroral breakups. Corresponding signatures were observed in five THEMIS satellites located between 8 and $24 R_E$ down the tail. Our results are summarized as follows.

1. Auroral breakup and NENL formation tended to repeat on a time scale of 10 min. We inferred that this was caused by interaction between the magnetic pileup region and NENL.
2. The second breakup was accompanied by a flow reversal, indicating a tailward retreat of the reconnection site. In addition, the third breakup included auroral activations near the nominal PCB latitude, a reconnection earthward flow, and energetic ions (~ 1 MeV), indicating that the Hones poleward leap phenomenon occurred, including another tailward retreat. Therefore, the tailward retreat occurred in a stepwise manner.
3. Spatially stepwise auroral poleward expansions were accompanied by the stepwise tailward retreat of the reconnection site. Both signatures were interpreted to be consequences of the tailward shift of the magnetic pileup region. Such stepwise development would be evident during northward IMF.
4. The stepwise tailward retreat resolved objections to the Hones poleward leap concept, which originally included only one tailward retreat. The poleward leap phenomenon includes a late auroral breakup involving the open magnetic field lines in the ionosphere. We propose the recognition of the poleward leap as full substorm development, well after the beginning of lobe field reconnection.
5. Fast flows were not observed with the Akasofu initial brightening but with auroral breakup; thus, NENL may have been quite localized or had not yet fully developed at the time of the Akasofu substorm onset.
6. Slow magnetic field-aligned earthward flows were observed before the first breakup, near the times of the precursory and Akasofu initial brightenings. The implications of this parallel flow remain unclear, but may be associated with the initial stage of reconnection or with localized plasma sheet thinning.
7. The connection between the onset arc in the premidnight and the two arcs in the postmidnight changed when the Akasofu initial brightening and the auroral breakup occurred. These observations suggest that the Akasofu initial brightening and the auroral breakup were not continuous but distinct.

References

- Aikio, A. T., T. Pitkanen, A. Kozlovsky, and O. Amm (2006), Method to locate the polar cap boundary in the nightside ionosphere and application to a substorm event, *Ann. Geophys.*, *24*(7), 1905–1917.
- Akasofu, S.-I. (1964), The development of the auroral substorm, *Planet. Space Sci.*, *12*(4), 273–282, doi:10.1016/0032-0633(64)90151-5.
- Alexandrova, A., R. Nakamura, V. S. Semenov, and T. K. M. Nakamura (2015), Motion of reconnection region in the Earth's magnetotail, *Geophys. Res. Lett.*, *42*, 4685–4693, doi:10.1002/2015GL064421.
- Angelopoulos, V. (2008), The THEMIS mission, *Space Sci. Rev.*, *141*(1–4), 5–34, doi:10.1007/s11214-008-9336-1.
- Angelopoulos, V., et al. (1996), Tailward progression of magnetotail acceleration centers: Relationship to substorm current wedge, *J. Geophys. Res.*, *101*(A11), 24,599–24,619, doi:10.1029/96JA01665.

- Angelopoulos, V., A. Runov, X. Z. Zhou, D. L. Turner, S. A. Kiehas, S. S. Li, and I. Shinohara (2013), Electromagnetic energy conversion at reconnection fronts, *Science*, *341*(6153), 1478–1482, doi:10.1126/science.1236992.
- Anger, C. D., and J. S. Murphree (1976), *ISIS-2 Satellite Imagery and Auroral Morphology*, pp. 223–234, Magnetospheric Particles and Fields, Netherlands.
- Artemyev, A. V., I. Y. Vasko, V. N. Lutsenko, and A. A. Petrukovich (2014), Formation of the high-energy ion population in the Earth's magnetotail: Spacecraft observations and theoretical models, *Ann. Geophys.*, *32*(10), 1233–1246, doi:10.5194/angeo-32-1233-2014.
- Atkinson, G. (1966), A theory of polar substorms, *J. Geophys. Res.*, *71*(21), 5157–5164.
- Auster, H. U., et al. (2008), The THEMIS fluxgate magnetometer, *Space Sci. Rev.*, *141*(1–4), 235–264, doi:10.1007/s11214-008-9365-9.
- Baker, D. N., R. D. Belian, P. R. Higbie, and E. W. Hones (1979), High-energy magnetospheric protons and their dependence on geomagnetic and inter-planetary conditions, *J. Geophys. Res.*, *84*(NA12), 7138–7154, doi:10.1029/JA084iA12p07138.
- Baker, D. N., T. I. Pulkkinen, V. Angelopoulos, W. Baumjohann, and R. L. McPherron (1996), Neutral line model of substorms: Past results and present view, *J. Geophys. Res.*, *101*(A6), 12,975–13,010, doi:10.1029/95JA03753.
- Baker, D. N., et al. (2002), Timing of magnetic reconnection initiation during a global magnetospheric substorm onset, *Geophys. Res. Lett.*, *29*(24), 2190, doi:10.1029/2002GL015539.
- Baumjohann, W., M. Hesse, S. Kokubun, T. Mukai, T. Nagai, and A. A. Petrukovich (1999), Substorm dipolarization and recovery, *J. Geophys. Res.*, *104*(A11), 24,995–25,000, doi:10.1029/1999JA00282.
- Birn, J., A. V. Artemyev, D. N. Baker, M. Echim, M. Hoshino, and L. M. Zelenyi (2012), Particle acceleration in the magnetotail and aurora, *Space Sci. Rev.*, *173*(1–4), 49–102, doi:10.1007/s11214-012-9874-4.
- Cao, X., et al. (2012), On the retreat of near-Earth neutral line during substorm expansion phase: A THEMIS case study during the 9 January 2008 substorm, *Ann. Geophys.*, *30*(1), 143–151, doi:10.5194/angeo-30-143-2012.
- Cheng, C. Z., and A. T. Y. Lui (1998), Kinetic ballooning instability for substorm onset and current disruption observed by AMPTE/CCE, *Geophys. Res. Lett.*, *25*(21), 4091–4094, doi:10.1029/1998GL900093.
- Chu, X., R. L. McPherron, T.-S. Hsu, V. Angelopoulos, Z. Pu, Z. Yao, H. Zhang, and M. Connors (2015), Magnetic mapping effects of substorm currents leading to auroral poleward expansion and equatorward retreat, *J. Geophys. Res. Space Physics*, *120*, 253–265, doi:10.1002/2014JA020596.
- Coppi, B., G. Laval, and R. Pellat (1966), Dynamics of geomagnetic tail, *Phys. Rev. Lett.*, *16*(26), 1207–1210, doi:10.1103/PhysRevLett.16.1207.
- Craven, J. D., and L. A. Frank (1987), Latitudinal motions of the aurora during substorms, *J. Geophys. Res.*, *92*(A5), 4565–4573, doi:10.1029/JA092iA05p04565.
- Donovan, E., et al. (2006), The THEMIS all-sky imaging array—System design and initial results from the prototype imager, *J. Atmos. Sol. Terr. Phys.*, *68*(13), 1472–1487, doi:10.1016/j.jastp.2005.03.027.
- Drake, J. F., M. Swisdak, K. M. Schoeffler, B. N. Rogers, and S. Kobayashi (2006), Formation of secondary islands during magnetic reconnection, *Geophys. Res. Lett.*, *33*, L13105, doi:10.1029/2006GL025957.
- Eastwood, J. P., et al. (2005), Observations of multiple X-line structure in the Earth's magnetotail current sheet: A Cluster case study, *Geophys. Res. Lett.*, *32*, L11105, doi:10.1029/2005GL022509.
- Eastwood, J. P., T. D. Phan, M. Oieroset, and M. A. Shay (2010), Average properties of the magnetic reconnection ion diffusion region in the Earth's magnetotail: The 2001–2005 Cluster observations and comparison with simulations, *J. Geophys. Res.*, *115*, A08215, doi:10.1029/2009JA014962.
- Elphinstone, R. D., J. S. Murphree, D. J. Hearn, W. Heikkilä, M. G. Henderson, L. L. Cogger, and I. Sandahl (1993), The auroral distribution and its mapping according to substorm phase, *J. Atmos. Terr. Phys.*, *55*(14), 1741–1762, doi:10.1016/0021-9169(93)90142-I.
- Elphinstone, R. D., et al. (1995), The double oval UV auroral distribution, 1. Implications for the mapping of auroral arcs, *J. Geophys. Res.*, *100*(A7), 12,075–12,092, doi:10.1029/95JA00326.
- Elphinstone, R. D., J. S. Murphree, and L. L. Cogger (1996), What is a global auroral substorm?, *Rev. Geophys.*, *34*(2), 169–232, doi:10.1029/96RG00483.
- Finlay, C. C., et al. (2010), International geomagnetic reference field: The eleventh generation, *Geophys. J. Int.*, *183*(3), 1216–1230, doi:10.1111/j.1365-246X.2010.04804.x.
- Hesse, M., and J. Birn (1991), On dipolarization and its relation to the substorm current wedge, *J. Geophys. Res.*, *96*(A11), 19,417–19,426, doi:10.1029/91JA01953.
- Hones, E. W. (1979), Transient phenomena in the magnetotail and their relation to substorms, *Space Sci. Rev.*, *23*(3), 393–410.
- Hones, E. W. (1986), The poleward leap of the auroral electrojet as seen in auroral images – Reply, *J. Geophys. Res.*, *91*(A5), 5881–5884, doi:10.1029/JA091iA05p05881.
- Hones, E. W. (1992), Poleward leaping auroras, the substorm expansive and recovery phases and the recovery of the plasma sheet, in *The International Conference on Substorms (ICS-1)*, Kiruna, Sweden, 23–27 March 1992, pp. 477–483, Eur. Space Agency Spec. Publ., Paris, France.
- Hones, E. W., J. R. Asbridge, S. J. Bame, and S. Singer (1973), Substorm variations of magnetotail plasma sheet from $X_{SM} \approx -6R_E$ to $X_{SM} \approx -60R_E$, *J. Geophys. Res.*, *78*(1), 109–132, doi:10.1029/JA078i001p0109.
- Hones, E. W., et al. (1984), Structure of the magnetotail at $220 R_E$ and its response to geomagnetic activity, *Geophys. Res. Lett.*, *11*(1), 5–7, doi:10.1029/GL011i001p00005.
- Hones, E. W., Jr. (1976), The magnetotail: Its generation and dissipation, *Phys. Sol. Planet. Environ.*, *2*, 558–571.
- Ieda, A., S. Machida, T. Mukai, Y. Saito, T. Yamamoto, A. Nishida, T. Terasawa, and S. Kokubun (1998), Statistical analysis of the plasmoid evolution with Geotail observations, *J. Geophys. Res.*, *103*(A3), 4453–4465.
- Ieda, A., D. H. Fairfield, T. Mukai, Y. Saito, S. Kokubun, K. Liou, C. I. Meng, G. K. Parks, and M. J. Brittacher (2001), Plasmoid ejection and auroral brightenings, *J. Geophys. Res.*, *106*(A3), 3845–3857, doi:10.1029/1999JA000451.
- Ieda, A., et al. (2008), Longitudinal association between magnetotail reconnection and auroral breakup based on Geotail and Polar observations, *J. Geophys. Res.*, *113*, A08207, doi:10.1029/2008JA013127.
- Imada, S., R. Nakamura, P. W. Daly, M. Hoshino, W. Baumjohann, S. Muehlbacher, A. Balogh, and H. Reme (2007), Energetic electron acceleration in the downstream reconnection outflow region, *J. Geophys. Res.*, *112*, A03202, doi:10.1029/2006JA011847.
- Iyemori, T. (1990), Storm-time magnetospheric currents inferred from midlatitude geomagnetic-field variations, *J. Geomag. Geoelectr.*, *42*(11), 1249–1265.
- Kadokura, A., A. S. Yukimatu, M. Ejiri, T. Oguti, M. Pinnock, and M. R. Hairston (2002), Detailed analysis of a substorm event on 6 and 7 June 1989: 1. Growth phase evolution of nightside auroral activities and ionospheric convection toward expansion phase onset, *J. Geophys. Res.*, *107*(A12), 1479, doi:10.1029/2001JA009127.
- Kamide, Y., and S. I. Akasofu (1974), Latitudinal cross section of the auroral electrojet and its relation to the interplanetary magnetic field polarity, *J. Geophys. Res.*, *79*(25), 3755–3771, doi:10.1029/JA079i025p03755.

- King, J. H., and N. E. Papitashvili (2005), Solar wind spatial scales in and comparisons of hourly Wind and ACE plasma and magnetic field data, *J. Geophys. Res.*, *110*, A02104, doi:10.1029/2004JA010649.
- Kisabeth, J. L., and G. Rostoker (1971), Development of polar electrojet during polar magnetic substorms, *J. Geophys. Res.*, *76*(28), 6815–6828, doi:10.1029/JA076i028p06815.
- Kisabeth, J. L., and G. Rostoker (1974), Expansive phase of magnetospheric substorms: 1. Development of auroral electrojets and auroral arc configuration during a substorm, *J. Geophys. Res.*, *79*(7), 972–984, doi:10.1029/JA079i007p00972.
- Liu, Y.-H., J. Birn, W. Daughton, M. Hesse, and K. Schindler (2014), Onset of reconnection in the near magnetotail: PIC simulations, *J. Geophys. Res. Space Physics*, *119*, 9773–9789, doi:10.1002/2014JA020492.
- Lyons, L. R., Y. Nishimura, B. Gallardo-Lacourt, Y. Zou, E. Donovan, S. Mende, V. Angelopoulos, J. M. Ruohoniemi, and K. McWilliams (2013), Westward traveling surges: Sliding along boundary arcs and distinction from onset arc brightening, *J. Geophys. Res. Space Physics*, *118*, 7643–7653, doi:10.1002/2013ja019334.
- Machida, S., Y. Miyashita, A. Ieda, M. Nosé, V. Angelopoulos, and J. P. McFadden (2014), Statistical visualization of the Earth's magnetotail and the implied mechanism of substorm triggering based on superposed-epoch analysis of THEMIS data, *Ann. Geophys.*, *32*(2), 99–111, doi:10.5194/angeo-32-99-2014.
- McFadden, J. P., C. W. Carlson, D. Larson, M. Ludlam, R. Abiad, B. Elliott, P. Turin, M. Marckwardt, and V. Angelopoulos (2008), The THEMIS ESA plasma instrument and in-flight calibration, *Space Sci. Rev.*, *141*(1–4), 277–302, doi:10.1007/s11214-008-9440-2.
- McPherron, R. L. (1991), Physical processes producing magnetospheric substorms and magnetic storms, in *Geomagnetism*, vol. 4, edited by J. Jacobs, pp. 594–739, Academic Press, London.
- Mende, S. B., H. U. Frey, S. P. Geller, and J. H. Doolittle (1999), Multistation observations of auroras: Polar cap substorms, *J. Geophys. Res.*, *104*(A2), 2333–2342, doi:10.1029/1998JA900084.
- Mende, S. B., S. E. Harris, H. U. Frey, V. Angelopoulos, C. T. Russell, E. Donovan, B. Jackel, M. Greffen, and L. M. Peticolas (2008), The THEMIS array of ground-based observatories for the study of auroral substorms, *Space Sci. Rev.*, *141*(1–4), 357–387, doi:10.1007/s11214-008-9380-x.
- Milan, S. E., J. A. Wild, B. Hubert, C. M. Carr, E. A. Lucek, J. M. Bosquad, J. F. Watermann, and J. A. Slavin (2006), Flux closure during a substorm observed by Cluster, Double Star, IMAGE FUV, SuperDARN, and Greenland magnetometers, *Ann. Geophys.*, *24*(2), 751–767.
- Miyashita, Y., et al. (2009), A state-of-the-art picture of substorm-associated evolution of the near-Earth magnetotail obtained from superposed epoch analysis, *J. Geophys. Res.*, *114*, A01211, doi:10.1029/2008JA013225.
- Moldwin, M. B., and W. J. Hughes (1993), Geomagnetic substorm association of plasmoids, *J. Geophys. Res.*, *98*(A1), 81–88, doi:10.1029/92JA02153.
- Nagai, T., et al. (1998), Structure and dynamics of magnetic reconnection for substorm onsets with Geotail observations, *J. Geophys. Res.*, *103*(A3), 4419–4440, doi:10.1029/97JA02190.
- Nagai, T., M. Fujimoto, R. Nakamura, W. Baumjohann, A. Ieda, I. Shinohara, S. Machida, Y. Saito, and T. Mukai (2005), Solar wind control of the radial distance of the magnetic reconnection site in the magnetotail, *J. Geophys. Res.*, *110*, A09208, doi:10.1029/2005JA011207.
- Nagai, T., I. Shinohara, M. Fujimoto, A. Matsuoka, Y. Saito, and T. Mukai (2011), Construction of magnetic reconnection in the near-Earth magnetotail with Geotail, *J. Geophys. Res.*, *116*, A04222, doi:10.1029/2010JA016283.
- Nakamura, R., W. Baumjohann, M. Brittnacher, V. A. Sergeev, M. Kubyshkina, T. Mukai, and K. Liou (2001), Flow bursts and auroral activations: Onset timing and foot point location, *J. Geophys. Res.*, *106*(A6), 10,777–10,789, doi:10.1029/2000JA000249.
- Nakamura, R., et al. (2011), Flux transport, dipolarization, and current sheet evolution during a double-onset substorm, *J. Geophys. Res.*, *116*, A00136, doi:10.1029/2010JA015865.
- Nishida, A., and N. Nagayama (1973), Synoptic survey for neutral line in magnetotail during substorm expansion phase, *J. Geophys. Res.*, *78*(19), 3782–3798, doi:10.1029/JA078i019p03782.
- Nishida, A., M. Scholer, T. Terasawa, S. J. Bame, G. Gloeckler, E. J. Smith, and R. D. Zwickl (1986), Quasi-stagnant plasmoid in the middle tail: A new preexpansion phase phenomenon, *J. Geophys. Res.*, *91*(A4), 4245–4255, doi:10.1029/JA091iA04p04245.
- Nosé, M., et al. (2012), Wp index: A new substorm index derived from high-resolution geomagnetic field data at low latitude, *Space Weather*, *10*, S08002, doi:10.1029/2012SW000785.
- Ohtani, S., R. Yamaguchi, M. Nosé, H. Kawano, M. Engebretson, and K. Yumoto (2002), Quiet time magnetotail dynamics and their implications for the substorm trigger, *J. Geophys. Res.*, *107*(A2), 1030, doi:10.1029/2001JA000116.
- Oka, M., et al. (2011), Magnetic reconnection X-line retreat associated with dipolarization of the Earth's magnetosphere, *Geophys. Res. Lett.*, *38*, L20105, doi:10.1029/2011GL049350.
- Opgenoorth, H. J., M. A. L. Persson, T. I. Pulkkinen, and R. J. Pellinen (1994), Recovery phase of magnetospheric substorms and its association with morning-sector aurora, *J. Geophys. Res.*, *99*(A3), 4115–4129, doi:10.1029/93JA01502.
- Pu, Z. Y., et al. (2010), THEMIS observations of substorms on 26 February 2008 initiated by magnetotail reconnection, *J. Geophys. Res.*, *115*, A02212, doi:10.1029/2009JA014217.
- Pytte, T., R. L. McPherron, M. G. Kivelson, H. I. West, and E. W. Hones (1976a), Multiple-satellite studies of magnetospheric substorms: Radial dynamics of plasma sheet, *J. Geophys. Res.*, *81*(34), 5921–5933, doi:10.1029/JA081i034p05921.
- Pytte, T., R. L. McPherron, and S. Kokubun (1976b), Ground signatures of expansion phase during multiple onset substorms, *Planet. Space Sci.*, *24*(12), 1115–1132, doi:10.1016/0032-0633(76)90149-5.
- Richmond, A. D. (1995), Ionospheric electrodynamics using magnetic apex coordinates, *J. Geomag. Geoelectr.*, *47*(2), 191–212.
- Rostoker, G. (1986), Comment on "The poleward leap of the auroral electrojet as seen in auroral images", *J. Geophys. Res.*, *91*(A5), 5879–5880, doi:10.1029/JA091iA05p05879.
- Rostoker, G., S. I. Akasofu, J. Foster, R. A. Greenwald, Y. Kamide, K. Kawasaki, A. T. Y. Lui, R. L. McPherron, and C. T. Russell (1980), Magnetospheric substorms—Definition and signatures, *J. Geophys. Res.*, *85*(NA4), 1663–1668, doi:10.1029/JA085iA04p01663.
- Russell, C. T. (2000), How northward turnings of the IMF can lead to substorm expansion onsets, *Geophys. Res. Lett.*, *27*(20), 3257–3259, doi:10.1029/2000GL011910.
- Russell, C. T., and R. L. McPherron (1973), The magnetotail and substorms, *Space Sci. Rev.*, *15*(2–3), 205–266.
- Russell, C. T., P. J. Chi, D. J. Dearborn, Y. S. Ge, B. Kuo-Tiong, J. D. Means, D. R. Pierce, K. M. Rowe, and R. C. Snare (2008), THEMIS ground-based magnetometers, *Space Sci. Rev.*, *141*(1–4), 389–412, doi:10.1007/s11214-008-9337-0.
- Saito, M. H., Y. Miyashita, M. Fujimoto, I. Shinohara, Y. Saito, K. Liou, and T. Mukai (2008), Ballooning mode waves prior to substorm-associated dipolarizations: Geotail observations, *Geophys. Res. Lett.*, *35*, L07103, doi:10.1029/2008GL033269.
- Sergeev, V. A., and A. G. Yahnin (1979), Features of auroral bulge expansion, *Planet. Space Sci.*, *27*(12), 1429–1440, doi:10.1016/0032-0633(79)90089-8.
- Sergeev, V. A., V. Angelopoulos, and R. Nakamura (2012), Recent advances in understanding substorm dynamics, *Geophys. Res. Lett.*, *39*, L05101, doi:10.1029/2012GL050859.

- Shiokawa, K., W. Baumjohann, and G. Haerendel (1997), Braking of high-speed flows in the near-Earth tail, *Geophys. Res. Lett.*, *24*(10), 1179–1182, doi:10.1029/97GL01062.
- Shiokawa, K., et al. (1998), High-speed ion flow, substorm current wedge, and multiple Pi 2 pulsations, *J. Geophys. Res.*, *103*(A3), 4491–4507, doi:10.1029/97JA01680.
- Sitnov, M. I., V. G. Merkin, M. Swisdak, T. Motoba, N. Buzulukova, T. E. Moore, B. H. Mauk, and S. Ohtani (2014), Magnetic reconnection, buoyancy, and flapping motions in magnetotail explosions, *J. Geophys. Res. Space Physics*, *119*, 7151–7168, doi:10.1002/2014JA020205.
- Slavin, J. A., M. F. Smith, E. L. Mazur, D. N. Baker, E. W. Hones, T. Iyemori, and E. W. Greenstadt (1993), ISEE 3 observations of traveling compression regions in the Earth's magnetotail, *J. Geophys. Res.*, *98*(A9), 15,425–15,446, doi:10.1029/93JA01467.
- Slavin, J. A., et al. (2002), Simultaneous observations of earthward flow bursts and plasmoid ejection during magnetospheric substorms, *J. Geophys. Res.*, *107*(A7), 1106, doi:10.1029/2000JA003501.
- Slavin, J. A., et al. (2003), Geotail observations of magnetic flux ropes in the plasma sheet, *J. Geophys. Res.*, *108*(A1), 1015, doi:10.1029/2002JA009557.
- Tsyganenko, N. A., and D. H. Fairfield (2004), Global shape of the magnetotail current sheet as derived from Geotail and Polar data, *J. Geophys. Res.*, *109*(A3), A03218, doi:10.1029/2003JA010062.
- Tsyganenko, N. A., and D. P. Stern (1996), Modeling the global magnetic field of the large-scale Birkeland current systems, *J. Geophys. Res.*, *101*(A12), 27,187–27,198, doi:10.1029/96JA02735.
- Ueno, G., S. Machida, T. Mukai, Y. Saito, and A. Nishida (1999), Distribution of X-type magnetic neutral lines in the magnetotail with Geotail observations, *Geophys. Res. Lett.*, *26*(22), 3341–3344, doi:10.1029/1999GL010714.
- Ueno, G., S. Ohtani, T. Mukai, Y. Saito, and H. Hayakawa (2003), Hall current system around the magnetic neutral line in the magnetotail: Statistical study, *J. Geophys. Res.*, *108*(A9), 1347, doi:10.1029/2002JA009733.
- Wiens, R. G., and G. Rostoker (1975), Characteristics of development of westward electrojet during expansive phase of magnetospheric substorms, *J. Geophys. Res.*, *80*(16), 2109–2128, doi:10.1029/JA080i016p02109.